A Remarkable Three Hour Thermonuclear Burst From 4U 1820-30

Tod E. Strohmayer

Laboratory for High Energy Astrophysics, NASA's Goddard Space Flight Center, Greenbelt, MD 20771

stroh@clarence.gsfc.nasa.gov

and

Edward F. Brown

University of Chicago, Enrico Fermi Institute, 5640 South Ellis Avenue, Chicago, IL 60637

brown@flash.uchicago.edu

ABSTRACT

We present a detailed observational and theoretical study of a $\sim$ 3 hr long X-ray burst (the "super burst") observed by the Rossi X-ray Timing Explorer (RXTE) from the low mass X-ray binary (LMXB) 4U 1820-30. This is the longest X-ray burst ever observed from this source, and perhaps one of the longest ever observed in great detail from any source. We show that the super burst is thermonuclear in origin. Its peak luminosity of $\sim 3.4 \times 10^{38}$ ergs s^{-1} is consistent with the helium Eddington limit for a neutron star at $\sim$ 7 kpc, as well as the peak luminosity of other, shorter, thermonuclear bursts from the same source. The super burst begins in the decaying tail of a more typical ($\approx$ 20 s duration) thermonuclear burst. These shorter, more frequent bursts are well known helium flashes from this source. The level of the accretion driven flux as well as the observed energy release of upwards of 1.5×10^{42} ergs indicate that helium could not be the energy source for the super burst. We outline the physics relevant to carbon production and burning on helium accreting neutron stars and present calculations of the thermal evolution and stability of a carbon layer and show that this process is the most likely explanation for the super burst. Ignition at the temperatures in the deep carbon "ocean" requires > 30 times the mass of carbon inferred from the observed burst energetics unless the He flash is able to trigger a deflagration from a much smaller mass of carbon. We show, however, that for large columns of accreted carbon fuel, a substantial fraction of the energy

released in the carbon burning layer is radiated away as neutrinos, and the heat that is conducted from the burning layer in large part flows inward, only to be released on timescales longer than the observed burst. Thus the energy released during the event possibly exceeds that observed in X-rays by more than a factor of ten, making the scenario of burning a large mass of carbon at great depths consistent with the observed fluence without invoking any additional trigger. A strong constraint on this scenario is the recurrence time: to accrete an ignition column of 10^{13} g cm^{-2} takes $\sim 13/(\dot{M}/3 \times 10^{17}$ g s$^{-1})$ yr. Spectral analysis during the super burst reveals the presence of a broad emission line between $5.8 - 6.4$ keV and an edge at $8 - 9$ keV likely due to reflection of the burst flux from the inner accretion disk in 4U 1820-30. We believe this is the first time such a signature has been unambiguously detected in the spectrum of an X-ray burst.

Subject headings: stars: neutron - stars: individual (4U 1820-30) - X-rays: bursts - X-rays: binaries - nuclear reactions, nucleosynthesis

1. Introduction

With an orbital period of only 11.4 minutes, 4U 1820-30 is the most compact low mass X-ray binary (LMXB) known (Stella et al. 1987). Thermonuclear X-ray bursts were discovered from this source by Grindlay & Gursky (1976) and attest that the primary is a neutron star. Using Vela 5B data Priedhorsky & Terrell (1984) found a 176 day periodic modulation of the X-ray flux from 4U 1820-30. Bursts have only been observed when the accretion driven flux is near the low end of its observed range, $< 4 \times 10^{-9}$ ergs cm^{-2} s^{-1}. Mass transfer in this system can be driven by gravitational radiation at the rate of $\sim 3 \times 10^{17}$ g s^{-1}. The binary resides in the globular cluster NGC 6624. Optical observations give a distance estimate of 7.6 kpc (Hesser & Shawl 1985; Rich, Minniti, & Liebert 1993). Based on the peak flux of photospheric radius expansion X-ray bursts, Vacca, Lewin, & van Paradijs (1986) estimated a likely distance of $\sim$ 6.6 kpc. The compact nature of the system requires that the secondary be a low mass helium dwarf (see Rappaport et al. 1987), so that the accreted material likely has a very high helium abundance. The observation of photospheric radius expansion bursts is consistent with the idea that helium flashes are the primary fuel for the 10–20 s duration bursts most commonly observed. Modulations of the UV flux from 4U 1820-30 at the 11.4 minute orbital period were predicted by Arons & King (1993) and subsequently discovered by Anderson et al. (1997). The UV modulations result from X-ray heating of the secondary and constrain the system inclination i to the range $35° \leq i \leq 50°$.

Smale et al. (1997) reported the discovery of kilohertz quasiperiodic oscillations (QPO)

from 4U 1820-30. Since then further observations have revealed that the highest observed kHz QPO appear to reach a saturation frequency near 1,050 Hz, suggesting the presence of a last stable circular orbit as predicted by General Relativity (GR) (Zhang, Strohmayer & Swank 1998; Kaaret, Ford & Chen 1998). If this hypothesis is correct it also suggests that the neutron star in 4U 1820-30 may be as massive as $\sim 2M_\odot$ (see also Arons & King 1993). Constraints derived from the study of X-ray bursts can provide information on the neutron star mass and radius and thus might also provide a key test of these conclusions.

Recently, Cornelisse et al. (2000) reported the detection of a very long (~ 3.5 hr) burst from 4U 1735-44 with the Wide Field Camera (WFC) on *BeppoSAX*. Spectral softening in this burst led the authors to conclude that it was thermonuclear in origin. There have been other recent reports of very long thermonuclear bursts from LMXBs, for example, Heise, in 't Zand & Kuulkers (2000) report long bursts from KS 1731-260 and Serpens X-1, and Kuulkers (2001) recently identified a likely super burst from GX 3+1 in RXTE/ASM data. As part of a Rossi X-ray Timing Explorer (RXTE) AO3 observing program to try and detect X-ray bursts as well as study kHz QPO from 4U 1820-30, RXTE was observing the source on September 9, 1999 UT when a long, powerful X-ray burst was observed. This burst was $\sim 1,000$ times longer than the more frequent thermonuclear bursts seen from the source (see for example Haberl et al. 1987). In this paper, we show that this super burst was thermonuclear in origin and that it was most likely fueled by burning of carbon ashes produced by the stable burning of helium accreted onto the neutron star in 4U 1820-30. In this respect, 4U 1820-30 differs from the other five super burst sources, which accrete a hydrogen/helium mixture and therefore produce much less carbon (see Cumming & Bildsten 2001). A consequence of this is that the recurrence time for this source will be of the order of a decade, however, unless the carbon ignition is somehow "triggered."

A very brief summary of the analysis in this paper was previously presented by Strohmayer (2000). We also note that during the preparation of this paper a burst lasting several hours was observed during RXTE observations of 4U 1636-53 in support of RXTE proposal 50030 (PI: Strohmayer). An analysis of this burst will be presented elsewhere. The 4U 1636-53 event was independently found with the ASM by Wijnands (2001), who also found a similar event in the ASM archive which occurred ~ 5 years earlier.

The plan of this paper is as follows. In § 2 we present the observed temporal and spectral characteristics as well as the energetics of the super burst. In § 3 we discuss the implications of the discrete spectral components (line and edge) observed during the burst. Section 4 begins with a discussion of the production of carbon and the thermal structure of the "ocean." We assess the amount of carbon needed to produce a thermonuclear runaway and the evolution of the ensuing burst. We conclude in § 5 with a summary of our principal

findings.

2. The X-ray Super Burst: Observations

As mentioned above, 4U 1820-30 has a $\sim$ 178 day X-ray intensity modulation (Pried-horsky & Terrell 1984). The All-sky Monitor (ASM) on board RXTE has been monitoring the source for more than 5 years. Figure 1 shows a portion of the 2–12 keV ASM lightcurve of 4U 1820-30. The dips down into the lowest flux state occur approximately at the 178 day period. Our RXTE observations on MJD 51430 (Sep. 9, 1999 UTC, indicated by the vertical arrow in the figure) caught the source near its low flux state when bursts can be observed.

In the weeks prior to our observation RXTE had a malfunction in one of its antenna transponders which disabled one of the high-gain antennas with which RXTE telemeters data to the ground. Because of this antenna malfunction some data from our observation were unfortunately lost. For the Proportional Counter Array (PCA) we have only Standard1 and Standard2 data for the entire event. These data provide 2–90 keV time histories with 1/8 s temporal resolution (Standard1) and 16 s spectral accumulations across the 2–90 keV bandpass (Standard2), respectively. Although the PCA bandpass is nominally 2 - 90 keV, for these data almost all source counts are in the 2 - 40 keV band. We did obtain some high time resolution event mode data (sampling rate of 1/8192 Hz) but only for two time intervals in the decaying portion of the burst. Unfortunately, we lost the high time resolution data during the onset of the burst. We will investigate the timing properties of 4U 1820-30 at the time of the super burst in a subsequent publication.

2.1. General Description

The time history of the burst is shown in figure 2. The 2–90 keV PCA Standard1 lightcurve with 1/8 s time resolution is the higher time resolution histogram (left axis), while the (8–30)/(2–8) keV hardness ratio from Standard2 data is the lower resolution histogram (right axis). The burst was observed with 3 of the 5 proportional counter units (PCUs 0, 2, and 3) which comprise the PCA. Note that the time axis is logarithmic. The event began with a typical helium flash from 4U 1820-30 which extends from about 3–15 seconds in Figure 2. However, before this first burst dies away the super burst erupts and is still decaying away 10,000 s later when our observation ended. The event shows a clear 'precursor' after which the X-ray flux dropped completely to background for a few seconds. A similar, but much weaker precursor can be seen in the helium flash burst just prior to the onset of the

super burst. This behavior is characteristic of very powerful photospheric radius expansion bursts (see Hoffman et al. 1978; Tawara et al. 1984; Lewin, Vacca & Basinska 1984; van Paradijs et al. 1990). Note also the hardening of the spectrum following the precursor. This is characteristic of the contraction phase of a radius expansion burst. We found in the RXTE archive one additional example of a helium flash burst from 4U 1820-30. In figure 3 we compare this burst, observed on May 2, 1997 at 17:32:39 UTC, with the helium flash which preceded the super burst. This He burst was observed with all 5 PCUs, so in order to make a closer comparison we have scaled the observed count rate by 3/5. Figure 3 shows the lightcurve of each burst at 1/8 s resolution from the Standard1 data mode. There are several things of note: both the preburst count rates as well as the peak count rate during the burst are similar, and each burst has a precursor or 'double peak' which indicates photospheric radius expansion. The above features of the time profile, combined with the observed behavior of the hardness ratio, are consistent with a thermonuclear origin for both bursts. The much longer timescale of the super burst compared to the shorter, more frequent helium flashes suggests a larger reservoir of nuclear fuel released at much greater column depth below the surface. These considerations suggest that carbon and/or oxygen are the likely fuel sources for the super burst. Later, in § 4, we will explore this scenario in greater detail.

2.2. Spectral Analysis

We used the Standard2 data to investigate the X-ray spectrum both before and throughout the burst. For most of the burst we did not have spectral data in a high time resolution mode. This was unfortunate, but since the evolution timescale of this burst is much longer than a typical 10 s burst it was only a significant problem near the onset of the burst where the data suggest the black body temperature was changing on a timescale shorter than our 16 s accumulations.

Before investigating the burst spectrum we analyzed the spectrum of the persistent, accretion driven flux. We used the standard PCA background estimation software, PCABACK-EST, to determine the PCA detector background. For all the spectral results we used only the top layer of detectors 0, 2, and 3 of the PCA. We found that the persistent flux before the burst is well fit by a thermal bremsstrahlung model (bremss in XSPEC) with a temperature $kT_{brem} \sim 8$ keV and flux of 3.5×10^{-9} ergs cm^{-2} s^{-1}. Figure 4 shows the time history of the thermal bremsstrahlung temperature, kT_{brem} (top panel), and the derived 2–20 keV flux (bottom panel). At a distance of 6.6 kpc the observed flux corresponds to a luminosity of 1.8×10^{37}, consistent with previous measurements of the persistent luminosity when bursts

are often observed (Clark et al. 1977; Haberl et al. 1987).

In most published analyses of burst spectral evolution the spectrum is obtained by subtracting off an estimate of the spectrum of the preburst, accretion driven flux. This should be reasonable when the burst flux does not appreciably disturb the accretion flow, however, during powerful radius expansion bursts it may be that the burst driven wind and near-Eddington flux can substantially effect the accretion process (see, for example, Walker & Meszaros 1989). We investigated both subtracting off the preburst emission as a background and assuming that the accretion-driven flux is completely shut off by the burst. For the latter case we simply subtracted off the appropriate detector background estimated with PCABACKEST. In general we found that for the majority of the burst we were able to get better fits by subtracting off the preburst spectrum, so we will discuss our results using this method. The best fit parameter values showed modest quantitative differences ($< 10\%$) when estimated using the two different background assumptions, but all of our qualitative conclusions are robust in the sense that they were independent of which assumption we used for the background.

Because this burst is $\sim 1,000$ times longer than typical thermonuclear bursts the timescale on which the thermal continuum changes is also much longer. This makes it possible to obtain very high signal to noise spectra during intervals in which the black body temperature remains fairly constant. For example we were able to accumulate 64 s spectra throughout most of the burst and still obtain good fits to the continuum with single temperature black body models. The spectrum during the burst is indeed thermal, and evolves in a way which is entirely consistent with thermonuclear bursts of shorter duration.

We found that a black body model with photoelectric absorption (model wabs*bbodyrad in XSPEC) alone usually did not provide an acceptable fit in the statistical sense, however, non-thermal continua gave much worse fits. The residuals when fitting a black body function and photoelectric absorption strongly suggest the presence of an emission line near 6.4 keV as well as an absorption edge between 7–9 keV. To model these components we included a gaussian emission line as well as an edge in our spectral model (model wabs*(bbodyrad+gaus)*edge in XSPEC). With these components included we were able to obtain acceptable fits with χ^2 per degree of freedom ~ 1. Figure 5 shows the characteristic residuals near the peak of the burst when the gaussian line and edge are removed from the model. Shown are the residuals, data minus model, in units of standard deviations. These residuals appear to be qualitatively similar to those reported by van Paradijs et al. (1990) for a powerful burst from 4U 2127+11 in M15. Both the line and edge are strongly required to adequately model the data. Figure 6 shows the count rate spectrum and residuals from a typical fit near the peak of the burst including the line and edge components, and demon-

strates the quality of fit we can achieve with this model. In general we find that the gaussian line at ~ 6.4 keV has finite width and often an energy centroid significantly less than 6.4 keV, suggestive of a line produced by reflection from a relativistic accretion disk in 4U 1820-30. Day & Done (1991) had suggested that such a signature should be present in burst spectra, but to our knowledge this is the first compelling observational evidence for such an effect, and it opens up the prospect of probing directly the properties of accretion disks during long thermonuclear bursts. With the disk reflection mechanism in mind we also modeled the line as an Fe fluorescence feature from an accretion disk (model diskline in XSPEC). Since the absorption edge will also be broadened by motions in the disk, we also included a smeared edge in these fits (model smedge in XSPEC).

We obtained excellent fits with this model for most of the burst duration except for about 100 s after the precursor. During this interval the photosphere is extended and the black body temperature is evolving too quickly for the 16 s Standard2 accumulations to resolve. For this interval we would have greatly benefited from higher time resolution spectra. We summarize our investigation of the time evolution of the burst spectrum in figures 7, 8 and 9. Figure 7 shows the time history of the burst from the Standard1 data on a linear time axis. The vertical dashed lines denote the region in which we derived black body fits. The time evolution of the spectral parameters is shown in figures 8 and 9. In each case the timespan is that of the interval between the dashed vertical lines in figure 7. The derived black body flux, temperature, and inferred radius at 6.6 kpc are shown in figure 8. The evolution of the line and edge parameters is shown in figure 9. The evolution of the black body temperature and flux is very similar to that of other thermonuclear bursts, the only difference being that the timescale of the evolution is much longer. For comparison we also investigated the spectral evolution during the shorter, helium flash observed from 4U 1820-30 on May 2, 1997. The peak black body temperature of both bursts approaches ~ 3 keV, and the peak fluxes are also consistent. This leaves no doubt about the thermonuclear origin of the super burst.

The super burst from 4U 1820-30 provides a unique opportunity to try and use burst spectroscopy to constrain the radius of a neutron star. The fact that the source distance is reasonably well constrained, the accreted matter is likely pure helium, and the burst lasted so long–giving high signal to noise spectra–make such an effort well worthwhile. Our aim in this paper is to lay out the basic properties of the super burst and a likely mechanism for its production. It is beyond the scope of this paper to present a detailed spectroscopic study in an attempt to derive constraints on the neutron star radius, however, we can make some simple estimates using our black body spectral fits and previous calculations of pure helium, neutron star atmospheres. The spectrum of an X-ray burst is not expected to be strictly that of a black body. Many authors have investigated the effects of electron scattering on the spectrum of X-ray bursting atmospheres, which is the dominant opacity source under the

conditions typical during bursts (see for example, London, Taam & Howard 1986; Ebisuzaki 1987; Titarchuck 1994; Madej 1991; Madej 1997). What is found is that the observed color temperature (ie. the temperature derived by fitting a black body function) is higher (harder) than the actual effective temperature of the atmosphere by a factor which ranges from about 1.4 to 1.7 and is largely dependent on the local X-ray flux. This correction factor is usually referred to as the hardening factor. For example, Ebisuzaki & Nakamura (1988) provide analytic approximations for the hardening factors in X-ray bursting, pure helium atmospheres. These factors depend only on the ratio of the local flux to the Eddington flux. Using these hardening factors we can convert our measured color temperatures to effective temperatures and then infer the size of the neutron star using the formula;

$$f_\infty = R^2(1 - 2GM/c^2R)^{-1}\sigma_R T_{eff}^4/d^2 , \tag{1}$$

where f_∞, T_{eff}, σ_R, and d are the flux, effective temperature (both measured far from the neutron star), Stefan - Boltzmann constant, and the source distance, respectively. Here M and R are the gravitational mass and radius of the star, both measured at the stellar surface. Because of the general relativistic effects this expression does not directly give an estimate of the radius independent of the mass. We used the flux and temperature measurements summarized in Figure 8 along with the hardening factors from Ebisuzaki & Nakamura (1988) to evaluate the above expression (assuming a distance of 6.6 kpc). For each pair of flux - temperature measurements we get an estimate of the quantity,

$$g(M, R) = R(1 - 2GM/c^2R)^{-1/2} . \tag{2}$$

The mean value of $g(M, R)$ in these data is 18.3 km, which implies a mean radius range of 15.7 to 13.85 km for a mass range of 1.4 to 2 $M_\odot$. This range of radii is about a factor of two larger than that determined by Haberl & Titarchuk (1995) for 4U 1820-30. We will explore the implications of the super burst for the mass - radius relation in 4U 1820-30 in greater detail in a sequel.

2.3. Observed Burst Energetics

The peak flux of 6.5×10^{-8} ergs cm^{-2} s^{-1} during the super burst implies a peak isotropic luminosity of 3.4×10^{38} ergs s^{-1} at a distance of 6.6 kpc. A neutron star with a pure helium photosphere has an Eddington luminosity of $L_{\rm Edd} = 2.5 \times 10^{38}(M/M_\odot)(1 - 2.9644(M/M_\odot)/R_{\rm km})^{1/2}$ ergs s^{-1}, which for reasonable neutron star masses and radii is consistent with our inferred peak luminosity. To determine the total energy in the observable burst we integrated the flux vs time profile, linearly interpolating across the gaps. We find a total fluence of 2.7×10^{-4} ergs cm^{-2}. At a distance of 6.6 kpc this implies a total energy

release of 1.4×10^{42} ergs. We note that these numbers should be considered lower limits since when our observations ended the burst flux was still decaying away. Moreover, it is likely that a substantial fraction of the energy released in the carbon burning layer is emitted as neutrinos or conducted inward and only released on a timescale much longer than the observed burst (see our discussion in § 4.3). Nevertheless, the observed X-ray fluence is $\sim 1,000$ times greater than is released in a typical helium flash from 4U 1820-30 (Haberl et al. 1987). The basic physics of nuclear burning instabilities on neutron stars indicates that carbon and oxygen burning can in principle provide this amount of energy, but not helium (see for example Lamb & Lamb 1978).

3. Implications of the Spectral Line and Edge

Franco & Strohmayer (1999) reported evidence for a ~ 6.4 keV emission line during the expansion phase of the May 2, 1997 burst from 4U 1820-30 observed with RXTE. There have been several previous claims of absorption lines between 4 and 5 keV from several burst sources, but their reality and interpretation have been controversial (see for example Waki et al. 1984; Nakamura, Inoue, & Tanaka 1988; Magnier et al. 1989; Foster, Ross, & Fabian 1987; Madej 1989), and we note that these previous line claims have not been confirmed by subsequent observations, for example, with the Advanced Satellite for Cosmology and Astrophysics (ASCA).

Our results leave no doubt that emission lines consistent with Fe Kα fluorescence can be produced during X-ray bursts. What is the origin of these discrete spectral features? A number of authors have investigated line production mechanisms during X-ray bursts. Foster, Ross, & Fabian (1987) investigated the formation of Fe features in the spectrum of cooling X-ray bursts. Their models predict broad Kα emission features should be present along with a 'blend' of photoelectric edges near 9.1 keV. We see both a broad line and an edge during the super burst, features similar to those predicted by Foster, Ross, & Fabian (1987), however, the observed energies of the features are somewhat problematic for this interpretation because the inferred redshifts are uncomfortably small for what would be expected from a canonical neutron star. For example, when our observed black body temperature reaches a maximum, the inferred line centroid is about 6.2 keV (see figures 8 and 9). If this resulted from a redshift of a 6.9 keV line of hydrogen-like Fe, one would require a redshift $1 + z = (1 - 2.9644(M/M_\odot)/R_{km})^{-1/2} \approx 6.9/6.2 = 1.113$ which would imply a neutron star of radius 21.5 km for a mass of $1.4 M_\odot$. This is prohibitively large even for the stiffest estimated neutron star equations of state. One might argue that the neutron star photosphere is still extended, but the temperature is thought to peak when touchdown

of the photosphere has occurred. If the rest energy of the line were 6.7 keV then the problem is only exacerbated. It is possible, however, that because of the modest spectral resolution of these observations, the measured line centroid could be influenced by the choice of the continuum model, so these conclusions should still be considered cautiously.

As mentioned previously, Day & Done (1991) suggested that a disk reflection component could be detected in the spectrum of X-ray bursts, and that detection of the absorption edge could be used to probe the ionization state of the disk. We think this is the simplest interpretation of the discrete features we see in the burst spectra. The inferred line centroids, which range from ~ 5.8–6.4 keV are comfortably consistent with an origin in the inner accretion disk. Relativistic motions in the disk also broaden the line profile. Furthermore, the inferred edge energies of ~ 7.5–9 keV are also consistent with this picture. Changes in the inferred energy of the absorption edge also suggest corresponding changes in the ionization state of the disk. For example, the highest inferred edge energies correspond to the time when the black body flux and temperature were near their peaks, suggesting that the burst flux has a significant effect on the ionization state of the disk. The equivalent width of the ~ 6.4 keV line ranges from $\sim 70 - 200$ eV, but is typically about 130 eV. This is reasonably consistent with recent estimates derived from spectral modelling of reflection from X-ray illuminated disks (see for example, Li, Gu & Kahn 2001; Nayakshin & Kallman 2001; Ross, Fabian & Young 1999). In principle, if the energies of the emission line and edge are known then one can constrain the ionization state of the gas. Turner et al. (1992) tabulate the run of Fe K line and edge energies with ionization parameter in the context of Fe $K\alpha$ observations of Seyfert galaxies (see their Figure 2). Based on this compilation, our line and edge energies appear consistent with an ionization parameter ~ 100 near the peak of the super burst. The subsequent evolution of the edge and line energies through the burst appears consistent with a decreasing ionization parameter as the burst evolves. This seems sensible, since the ionizing flux (from the burst) is decreasing with time. However, more precise spectral modelling will be required to investigate the implications for disk structure in detail. This will be left for a future study.

During the decay of the burst there is a highly significant hardening of the spectrum (see figure 8, near 3000 s). This is evidenced by an increase in the black body temperature along with a decrease in the inferred black body radius. Even more interesting, the line flux and edge depth both decrease dramatically at the time of this spectral hardening (see figure 9). This behavior is somewhat reminiscent of state changes in other accreting X-ray binaries, but happens on a much shorter timescale. Perhaps the inner disk is transitioning to a hot, optically thin condition, similar to an ADAF (see for example Narayan, Yi, & Esin 1998). Alternatively, we could be seeing a geometric effect of something in the system shadowing the disk so that the reflected component is greatly reduced, perhaps a warp in the accretion

disk. Unfortunately, an Earth occultation interval blocks our view of what happens next. Also of note is the fact that shortly after this hardening episode chaotic dipping can be seen in the lightcurve for an extended period. Although for part of this time the source is Earth occulted, this dipping may be another indication of the accretion flow having been strongly affected by the burst.

Another possibility for the discrete components is that we are seeing fluorescence in the wind material blown off the star by the super-Eddington burst. In this case one might expect to see a correlation of the line strength with the amount of absorbing material along the line of sight, and this does not seem to be the case.

It seems likely that at some level all of these processes are at work, but it seems most plausible that disk reflection is the dominant mechanism. The UV modulations observed by Anderson et al. (1997) suggest the system has an inclination $\sim 45°$ (see Arons & King 1993), which would provide a favorable geometry for reflection. The energy resolution of the PCA is not sufficient to resolve the line and edge in detail. For example, a redshifted line from the neutron star photosphere could be obscured by the broad line produced by disk reflection. However, additional observations of such a burst with much higher spectral resolution could help distinguish amongst these different scenarios, and could provide us with a powerful new probe of the accretion process in LMXBs.

4. The Case for Unstable Carbon Burning

Having described the observation of the super burst and the evidence for it being thermonuclear in origin, we now examine its source of fuel and its ignition. In order for He burning to power the super burst, the accumulated He must not ignite until the base of the helium layer reaches densities of order 10^8 g cm^{-3} (e.g., Fryxell & Woosley 1982; Zingale et al. 2001). This can only occur if the atmosphere is extremely cold and in particular requires a local accretion rate $\lesssim 2 \times 10^{-11}$ $M_\odot$ yr^{-1} (Fryxell & Woosley 1982) in the absence of any heat flux from the core. Such low accretion rates are not consistent with the observed flux and the presence of concurrent He flashes. The fact that a helium flash went off just prior to the super burst also indicates that helium cannot be the primary energy source for the giant burst. We therefore discount the possibility that ^{4}He could be the fuel for the super burst.

As shown in the previous section, the spectral evolution of the burst is roughly consistent with the release of energy at large densities in the star. The burning of carbon to iron-peak elements releases $\approx 10^{18}$ erg g^{-1} so that at least 2×10^{24} g of carbon is needed

to account for the energy released in the burst (in § 4.3 we argue that this is likely an underestimate of the total burst energetics). An $M_C = 2 \times 10^{24}$ g mass of ^{12}C uniformly deposited over the surface of a neutron star of radius $R = 10$ km has a column density $y_C \approx M_C/4\pi R^2 \approx 1.6 \times 10^{11}$ g cm^{-2}. Hydrostatic balance gives the pressure at the base of the layer, $p = gy$; from the equation of state and the thermal conductivity (see § 4.3 for details) we may estimate the cooling timescale for a mass of newly formed ^{56}Fe to be $\sim C_p y^2/(\kappa \rho) \sim 10^3(y_C/10^{11}$ g cm$^{-2})^{3/4}$ s, roughly consistent with the observed thermal decay timescale of the burst. Here C_p is the specific heat, per unit mass, κ is the thermal conductivity, ρ is the density, and $y = \int_z^\infty \rho \, dz'$ is the column depth. If mass transfer is driven by gravitational radiation we expect an accretion rate of ~ 1–3×10^{17} g s$^{-1} \sim 5 \times 10^{-9} M_\odot$ yr^{-1} onto the neutron star; this level is also roughly consistent with the accretion rate required to account for the persistent luminosity of 1.8×10^{37} erg s^{-1}. The precise rate is uncertain because of our lack of knowledge concerning the efficiency with which gravitational energy is converted to X-ray flux. If this conversion were 100% efficient, then one would require $\dot{M} = 10^{17}$ g s^{-1} (assuming a 1.4 $M_\odot$ and 10 km neutron star); a more realistic number, however, is probably 5–20 %, so that the actual mass accretion rate could be higher than 10^{18} g s^{-1}.

Isotropic (over the stellar surface) accretion at a rate of 3×10^{17} g s^{-1} can deposit a sufficient amount of carbon to power the burst only after 0.2–0.6 yr, so such events should indeed be rare, consistent with only one such burst being observed from this source.

Unstable carbon burning on accreting neutron stars was conjectured by Woosley & Taam (1976) and studied by Taam & Picklum (1978), who found that for accretion rates of 10^{-10}–10^{-9} $M_\odot$ yr^{-1}, the timescale for recurrence would be of order 10–100 yr, with the bursts having an energy of order 10^{44} erg, about 100 times greater than that measured for this burst. While the original calculation of Taam & Picklum (1978) assumed accretion of hydrogen-rich material, recent calculations with large reaction networks for both unstable (Schatz et al. 2001) and steady-state burning (Schatz et al. 1999) find that only a small amount of ^{12}C is produced during hydrogen burning. For this reason, the scenario presented here (i.e., the ignition of a carbon-rich layer) is probably not relevant for the super bursts seen from 4U 1735-44, KS 1731-260, GX 3+1, Ser X-1 and 4U 1636-53, which are likely accreting a mix of hydrogen and helium (see Cornelisse et al. 2000; Heise, in 't Zand, & Kuulkers 2000; Kuulkers 2001; Wijnands 2001). The small amount of ^{12}C produced during rp-process burning might be a fuel for the other super-bursts; for a discussion of this possibility, we refer the interested reader to Cumming & Bildsten (2001).

While the burning of ^{12}C is a plausible cause of this super burst, the ignition of a pure carbon layer requires either high temperatures (Brown & Bildsten 1998) or a large mass of carbon (Taam & Picklum 1978). In this section, we address these constraints. We

begin (§ 4.1) by estimating the amount of carbon produced. We then (§ 4.2) investigate the conditions for ignition of a carbon-rich layer. We demonstrate, in the absence of a "trigger," that a much larger mass of ^{12}C is required than that estimated from the observed burst energetics. Section 4.3 provides a resolution to this dichotomy: namely, for very large bursts most of the heat is carried off by neutrinos, and of the heat conducted from the burning layer, a substantial amount flows *inward*, to be released on much longer timescales (days to weeks). The long timescale for thermal diffusion at great depths means that only a fraction of the total burst energy is radiated away in the few hours following the burst rise. A consequence of requiring a massive carbon layer for ignition is that the recurrence times of such super bursts will be many years.

4.1. The Production of ^{12}C

Whether or not ^{12}C is produced by the burning of ^{4}He depends largely on whether the burning is stable. The ashes of stable He burning are composed mostly of ^{12}C at the lowest accretion rates compatible with stability (Brown & Bildsten 1998). In contrast, unstable burning leads to much higher temperatures, which allow the reactions to run up to iron-peak nuclei. Numerical calculations find that for unstable burning only a trace amount of residual He is expected ($< 1\%$ by mass; Joss & Li 1980) and no ^{12}C. Because this source accretes nearly pure He, the endpoint of the unstable nucleosynthesis will be iron-peak nuclei, rather than the heavier species produced during mixed H/He burning.

The luminosity of this source is variable by a factor of ≈ 4 (Figure 1), and type I X-ray bursts are only observed when the luminosity is in its low state. The lack of unstable burning when the luminosity is high is somewhat puzzling, since the inferred accretion rate is still less than what is necessary for stability, according to linear analysis and time-dependent calculations (see Bildsten 1998, and references therein). One possibility is that the burning is unstable, but that the flame front propagates at the slow conductive velocity (Bildsten 1995). Whether such fronts can slowly propagate on a rapidly rotating neutron star is an open question (for a discussion, see Spitkovsky et al. 2001). Another possibility is that the accretion flow does not spread over the entire surface prior to He ignition, as suggested by Bildsten (2000) as an explanation for patterns of unstable hydrogen/helium burning on Z-sources. If the efficiency of conversion of gravitational energy to X-ray luminosity is modest, then the inferred accretion rate can be substantially higher, reducing the discrepancy between theory and observation.

One constraint on the amount of carbon produced would be the recurrence time of a super burst. We did search the RXTE/ASM archival lightcurve of 4U 1820-30 for additional

instances of super bursts, but did not find any. Although the ASM monitors the whole sky it does not do so all the time, so that the total time during which another super burst from 4U 1820-30 could have been seen is only about 25 days out of a time span of about 5 years. Since only one such event was seen and the total on source time was modest we can not place a strong constraint on the recurrence rate. It is unlikely to be much larger than 0.05 day^{-1}, but could easily be ten times lower than this. We note that the source is only at or below the ASM flux level at which thermonuclear bursts were observed for about 10% of the time. For the purposes of this paper, we take the absence of observed type I X-ray bursts during the episodes of high-luminosity as indication that ^{12}C is produced. Over each 178 day cycle, we estimate that roughly $(1/2) \times 178$ d $\times \dot{M} \approx 10^{24}$ g of ^{12}C is formed. As we describe in the next section, it is quite plausible that the iron made in the bursts mixes with the carbon made during stable burning, so that the deep ocean is a mixture of the two.

4.2. Ignition of the Carbon Layer

The physics involved in the ignition of the carbon layer is detailed in Brown & Bildsten (1998); here we review that discussion. The scale height is of order $1000(y/10^{11}$ g cm$^{-2})^{1/4}$ cm $\ll R$, so that the carbon layer is susceptible to a thin-shell instability (Hansen & Van Horn 1975), and we may neglect the variation of gravity with depth.

We compute the thermal structure of the carbon layer following the method outlined in Brown & Bildsten (1998). The relevant equations are those of continuity (for each species),

$$\frac{\partial X_j}{\partial t} + \mathbf{v} \cdot \nabla X_j = \frac{A_j}{N_A \rho}(-r_{\text{dest}}^{(j)} + r_{\text{prod}}^{(j)}), \tag{3a}$$

entropy,

$$T\frac{ds}{dt} = -\frac{1}{\rho}\nabla \cdot \mathbf{F} + \varepsilon, \tag{3b}$$

and flux,

$$\mathbf{F} = -\kappa \nabla T. \tag{3c}$$

Here X_j and A_j are the mass fraction and mass number of species j, $N_A = 6.02 \times 10^{23}$ g^{-1} is Avogadro's number, and $r_{\text{dest}}^{(j)}$ and $r_{\text{prod}}^{(j)}$ are the volumetric destruction and production rates of species j via nuclear reactions.

For the electron equation of state, we use a table interpolation scheme of the Helmholtz free energy (Timmes & Swesty 2000). The ionic equation of state includes Coulomb interactions, which are parameterized by $\Gamma \equiv (\langle Z \rangle e)^2/(a k_B T)$, where $4\pi a^3/3 = n_I^{-1}$ is the mean volume per ion. In this problem, Γ spans a range of values $\ll 1$ (ions are weakly coupled)

to > 173 (ions are crystalline; see Farouki & Hamaguchi 1993 and references therein). For $1 < \Gamma \lesssim 173$ the ions are in a liquid state, and we shall refer to this layer as the "ocean".

The thermal conductivity κ contains contributions from both radiative transport (in the diffusive approximation), and electronic thermal conduction. Radiative transport dominates at lower densities; in this regime we use the Rosseland mean of both Thompson scattering (with corrections for the relativistic, partially degenerate electrons; Sampson 1959; Buchler & Yueh 1976) and free-free absorption with an analytical approximation to the Elwert factor (Schatz et al. 1999), which reproduces the tabulated gaunt factor of Itoh et al. (1991). At higher densities electron conduction dominates; we include contributions from electron-electron scattering, for which we use the fit (Potekhin et al. 1997) to the calculations of Urpin & Yakovlev (1980), and electron-ion scattering, for which we use the fits of Potekhin et al. (1999). The treatment of Potekhin et al. (1999) is valid in both the liquid and crystalline phases.

We are interested in the unstable ignition of ^{12}C. Prior to ignition, the heating from $^{12}C + ^{12}C$ is negligible, and we do not include it in the thermal structure calculation. In the carbon ocean and iron crust, then, $\varepsilon = -\varepsilon_\nu$, the neutrino emissivity, for which we use the fits of Itoh et al. (1996) to the pair, plasma, photoneutrino, bremsstrahlung, and recombination rates. We change the composition discontinuously from a mixture of ^{12}C and ^{56}Fe (we allow for the possibility of a mixed layer) to ^{56}Fe at an interface column y_i, which is chosen to be roughly where we expect the ^{12}C to have ignited.

The thermal timescale, at a given column, is much faster than the timescale for accretion to supply that column of material. As a result, we may simplify our equations by presuming steady-state ($\partial_t \rightarrow 0$) and converting the structure equations (eq. [3a]–[3c]) from PDE's into ODE's. To further simplify calculations, we rewrite the equations with the column y as the independent variable, $\partial_z = -\rho \partial_y$, and neglect differential sedimentation of the ions. With these approximations, the velocity of the fluid is $\mathbf{v} = -\mathbf{e}_z \dot{m}/\rho$, where $\dot{m}$ is the accretion rate per unit area, and the structure equations reduce to

$$\frac{dX_{He}}{dy} = -\lambda_{3\alpha} \dot{m}^{-1} \tag{4a}$$

$$\frac{dX_C}{dy} = \lambda_{3\alpha} \dot{m}^{-1} \tag{4b}$$

$$\frac{dT}{dy} = \frac{F}{\rho \kappa} \tag{4c}$$

$$\frac{dF}{dy} = C_p \dot{m} \left(\frac{dT}{dy} - \frac{T}{y} \nabla_s \right) + \varepsilon. \tag{4d}$$

Here $\nabla_s \equiv (\partial \ln T / \partial \ln p)_s$ is the adiabatic gradient and $\lambda_{3\alpha} = \varepsilon_{3\alpha}/Q_{3\alpha}$, where $Q_{3\alpha} =$

7.274 MeV is the energy released per formed carbon. Equations (4a)–(4d) depend on both the surface gravity g (through $\rho(p = gy, T)$) and the local accretion rate $\dot{m}$. We fix $g = GM/R^2(1 - 2GM/Rc^2)^{-1/2}$ to the value 2.3×10^{14} cm s^{-2} appropriate for a neutron star of mass 1.4 $M_\odot$ and radius 10 km.

Because the accretion rate varies, we first fix the temperature of the deep crust by solving equations (4a)–(4d) at the mean accretion rate $\dot{m} = 2.25 \times 10^4$ g cm^{-2} s^{-1}, which roughly corresponds to the persistent mean accretion rate of the source if uniformly deposited over the surface. To fix the composition of the atmosphere and the bottom of the He-rich layer, we compute the burning of He to C via the 3α reaction. At low accretion rates, the ^{12}C$(\alpha, \gamma)^{16}$O reaction rate is negligible compared to the 3α rate (Bildsten 1995), and we therefore just track the abundances of ^{4}He and ^{12}C. For $\varepsilon_{3\alpha}$, the heating rate from the 3α reaction, we use the analytical fit of Fushiki & Lamb (1987).

Boundary conditions are specified at both ends of the computational domain. The thermal structure of the atmosphere is insensitive to the photosphere temperature (it is, roughly speaking, a radiative-zero solution) for $y \gg K^{-1}$, K being the opacity; for definiteness, we set $T = (GM\dot{M}/2R\sigma_{\rm R})^{1/4}$ at $y = 10^{2.5}$ g cm^{-2}, where $\sigma_{\rm R}$ is the Stefan-Boltzmann constant. The choice of boundary condition at the other end of the computational domain (set to $y = 10^{14}$ g cm^{-2}) is more problematic. The high thermal conductivity of the degenerate, relativistic electrons ensures that the ocean is well-coupled to the thermal state of the inner crust and core. Previous studies (e.g., Taam & Picklum 1978; Brown & Bildsten 1998) simply took the flux to be zero at the inner boundary. For an accreting neutron star, continual compression of the deep crust forces a series of electron captures, neutron emissions, and pycnonuclear reactions (Bisnovatyi-Kogan & Chechetkin 1979; Blaes et al. 1990; Haensel & Zdunik 1990); in steady-state, most of the heat released from these reactions flows into the core but a small amount ($\lesssim 0.1$ MeV per accreted nucleon for $\dot{M} \gtrsim 0.1 \dot{M}_{\rm Edd}$) flows outward (Brown 2000). The thermal timescale in the inner crust is of order years (Brown et al. 1998) and so the temperature there depends mostly on the time-averaged accretion rate. We therefore adjust the temperature at $\log(y) = 14.0$ so that the flux from the deep crust is $\approx 0.1 N_{\rm A}\dot{m}$ MeV.

With these approximations, we numerically integrate the equations (3a)–(3c) using a stiff ODE solver. We integrate from each boundary and iteratively adjust the flux at the upper and lower boundaries so that the temperature and flux are continuous at a fitting point. The result of this integration, over the range of y relevant for ignition, is shown in Figure 10. We show the temperature (*solid line*; left-side vertical axis) and flux in units of MeV per accreted nucleon (*dotted line*; right-side vertical axis). The arrow is to guide the eye and mark the value of $T(y = 10^{14}$ g cm$^{-2})$. The top axis shows the time required to accrete

a given column at $\dot{m} = 2.3 \times 10^4$ g cm^{-2} s^{-1}. As we shall explain momentarily, it is plausible that the carbon and iron form a mixed layer; we therefore change the mixture from ^{4}He/^{12}C to ^{12}C/^{56}Fe ($X_C = 0.3$) at $y = 10^{10}$ g cm^{-2}. The kink in the temperature at that point is because the conductivity decreases when we reset the composition. We chose $X_C = 0.3$ as a minimal case for ignition. A larger X_C would increase the ocean thermal conductivity and, for a fixed flux of 0.1 MeV$N_A\dot{m}$, lower the ocean temperature. This increases both the recurrence time and the total burst energetics (although, as we shall explain in the next section, a larger X_C will not increase the X-ray fluence substantially because the additional energy is lost to neutrinos). A smaller X_C may not ignite unstably (Cumming & Bildsten 2001). With a judicious use of hindsight, we set the base of the C/Fe layer at $y = 10^{13}$ g cm^{-2} (roughly where the ^{12}C will ignite); at greater column the composition is pure Fe. The point where the pure Fe layer begins is marked in Figure 10 by the large black dot.

As explained in Brown & Bildsten (1998), thermal conduction is more efficient at cooling the ocean than neutrino emission at these temperatures (Brown & Bildsten 1998). The condition for ignition is crudely expressed as $d\varepsilon_C/dt > d\varepsilon_{th}/dt$, where $\varepsilon_{th} = \rho\kappa T/y^2$ is an approximation to $\rho^{-1}\nabla \cdot \mathbf{F}$. For the heating ε_C, we use the rate of Caughlan & Fowler (1988) and incorporate strong screening using the formalism of Ogata et al. (1993). In Figure 10, we show the points where ignition occurs (*heavy dashed curve*). Note that the strong temperature sensitivity of the ^{12}C + ^{12}C reaction means that the location of this curve is relatively insensitive to the precise method of defining ignition. As is evident from the figure, the temperature in the carbon-rich layer is too cold, by about a factor of 2–3, for ignition to occur if the base of the carbon-rich layer is at $y = 10^{11}$ g cm^{-2}. The presence of heavy elements (e.g., ^{104}Ru) in the ocean of the other super burst sources makes the carbon-containing layer hotter, for a given flux from the crust and core, and allows for a smaller ignition column (Cumming & Bildsten 2001).

In this calculation, the mass of carbon at the depth where ignition occurs is $\approx 4\pi R^2 \times 0.3 \times 10^{13}$ g cm$^{-2} \approx 3.8 \times 10^{25}$ g. This is about a factor of 20 greater than that indicated by our estimate of the burst energetics. For a lesser X_C, the conductivity is lower and the temperature at which ignition occurs increases; as pointed out by Cumming & Bildsten (2001), however, the carbon burning will become stable at low accretion rates and small carbon abundances. Their estimate implies that for the conditions we assume here, $X_C \gtrsim 0.5$ is required for unstable ignition. Consistent with this estimate, we find that for this calculation the lifetime, $-X_C/\dot{X}_C$, is slightly less than the accretion timescale $y/\dot{m}$ at the ignition point. For this reason we do not consider smaller mass fractions of carbon.

The temperature at the base of the carbon layer is mostly determined by the flux flowing from deeper in the star. The reason is that the heat flowing from the crust (~ 0.1 MeV per

accreted nucleon) is larger than that generated by compressional heating ($\sim C_p T \nabla_s / N_A \sim$ 1 keV per accreted nucleon), and the high conductivity of the degenerate plasma enforces a very shallow temperature gradient. At the time of the super burst, the accretion rate was lower than the mean, and the deep ocean was slightly colder than in this calculation, making ignition even more difficult.

As mentioned earlier, locally high accretion rates onto a small portion of the stellar surface may be an explanation for the lack of bursts during the high-luminosity state of this source. At higher local accretion rates, the ignition column decreases. To heat a confined carbon column to ignition at $y = 10^{11}$ g cm^{-2} requires local accretion rates in excess of 5 times the local Eddington rate (Brown & Bildsten 1998). It is implausible, however, that the accreted matter would fail to spread over the surface prior to reaching this column. While strong magnetic fields ($\sim 10^{12}$ G) could possibly confine such a large column (Brown & Bildsten 1998; Litwin et al. 2001), there is no evidence, such as pulsations in the persistent emission, for such strong organized fields in this source.

What about heating of the carbon layer during a type I X-ray burst? The timescale to conduct the heat from the base of the He-rich layer to the surface is ~ 10 s (the decay timescale of the burst). Unlike in the degenerate ocean, the dominant opacity is Thompson scattering, for which the equivalent radiative conductivity is independent of depth. As a result, the inward propagation of heat is inefficient (as can be checked by a calculation similar to that described in equation (7) and the heating of the carbon layer is too small to force an ignition.

The fact that this source cyclically produces ^{12}C (in the high-luminosity) state and iron-peak elements (through unsteady He burning in the low-luminosity state) has some interesting consequences. During a He burst, the burning produces mostly ^{56}Fe. As the iron cools, it becomes denser than the underlying carbon, because the iron has fewer electrons per nucleon than helium. The base of the unstable He burning layer is therefore susceptible to first a secular salt-finger and then a Rayleigh-Taylor instability. For example, at an interface pressure of 2×10^{23} dyn cm^{-2} and a ^{12}C temperature of 2.5×10^8 K, the iron layer is less dense than the carbon layer only when its temperature is $> 7.6 \times 10^8$ K.

Terrestrial Rayleigh-Taylor experiments and numerical simulations (Youngs 1994, and references therein) suggest that the time t for the interface (between fluids of density ρ and ρ') to traverse a distance s is given by $t = [s/(\alpha \mathcal{A} g)]^{1/2}$, where $\mathcal{A} = (\rho - \rho')/(\rho + \rho')$ is the Atwood number and $\alpha \approx 0.03$ is uncertain by a factor of 2. Taking s to be a scale height, we find that for this case $t \sim 10^{-4}$ s. Thermal diffusion is ineffective on this timescale; the characteristic distance over which heat can diffuse on this timescale is less than 1 cm, which is much smaller than the pressure scale height (~ 1000 cm). The scaling of distance with t^2

comes about because of mergers between falling spikes into larger and larger drops; in the case of a stratified medium, this effect is counteracted to some extent by compression of the falling spikes. As the iron "plume" descends, the ambient medium (carbon) is entrained, reducing the buoyancy contrast and eventually halting its descent (Townsend 1966).

Because the mass of Fe available after a He burst is much less than the mass of the carbon-rich layer, it is unlikely that the sinking Fe will fall to the base of the carbon-rich layer. Whether a descending plume would be able to spark an ignition of the carbon layer at $y \ll 10^{11}$ g cm^{-2}, and whether a flame could propagate without quenching at those lower densities, is unknown. In any case, it is likely that at least some of the iron is mixed into the carbon layer and advected deeper into the star by continual accretion, so that ignition will occur in a mixed C/Fe layer, as we have assumed. Detailed calculations are outside the scope of this paper; for now we leave this as an interesting possibility.

4.3. Evolution of the Burst

As noted above, the ignition of ^{12}C, for conditions relevant to this source, requires either a large accumulated column of carbon-rich material, or a trigger, perhaps associated with an earlier He flash. In this subsection, we explore the evolution of an unstable ignition at $y = 10^{13}$ g cm^{-2} of a C/Fe layer ($X_C = 0.3$). Unlike for normal (10–20 s duration) type I X-ray bursts, the energetics of this super burst are much greater than that inferred from the X-ray lightcurve. There are two reasons for this. The first is that neutrino cooling is more efficient than thermal conduction at the peak temperature ($> 5 \times 10^9$ K) reached in the burst. The second reason is that thermal conduction into deeper layers is efficient and competes with the outward thermal transport. Because of the great depth of ignition, the thermal time is of order 10^5 s and is much longer than the duration of the observation. We now consider each of these cooling mechanisms in turn.

Once the instability begins, the heating timescale $C_p T / \varepsilon_C$ is, by definition, shorter than both the thermal conduction and neutrino cooling timescales. At first the nuclear burning timescale is comparable to the thermal conduction time ($\gtrsim 10^4$ s; Taam & Picklum 1978), but it accelerates with increasing temperature. We calculate the peak temperature from the equation $\int_{T_i}^{T_p} C_p \, dT = X_C E_{\text{nuc}}$, where $E_{\text{nuc}} \approx 10^{18}$ erg g^{-1} is the energy per gram released in burning ^{12}C to Fe-peak elements. For a pure carbon layer, the temperature would reach $T_p \approx 1.5 \times 10^{10}$ K if all the carbon burned to iron. Note that even at this extreme temperature, the electrons are still (mildly) degenerate; the Fermi energy is ≈ 5 MeV. In addition, the radiation pressure, at this temperature, is only 1.3×10^{26} dyn cm^{-2}, about a tenth of the total. Unlike in He burning, the peak temperature is therefore not limited by the expansion

of the burning layer if the base of that layer is sufficiently deep. Because of the high density, photodisintegration reactions are also unimportant until temperatures in excess of 10^{10} K are reached, as can be checked by a Saha-type equation. For the abundance ($X_C = 0.3$) used in Figure 10, $T_p = 9.1 \times 10^9$ K.

Although neutrino cooling is unimportant for stabilizing the ignition of carbon on a neutron star (Brown & Bildsten 1998), it is more efficient than thermal conduction when the burning layer is at its peak temperature[1]. In addition, thermal conduction to the surface is more efficient at lower column and competes more effectively with neutrino cooling. For a very deep layer, however, the situation is different. The thermal conduction timescale is longer and the peak temperature reached is much higher. To investigate the cooling, we constructed a one-zone approximation of the layer following the burning,

$$C_p \frac{\partial T}{\partial t} = -\frac{\rho \kappa T}{y^2} - \epsilon_\nu.$$

(5)

We set the initial temperature at $T_p(X_C)$ but switched the composition to Fe to simulate the ashes. At a temperature $\sim 10^{10}$ K, the dominant neutrino-producing process is from electron-positron pairs. As a result, the neutrino emissivity *decreases* as density increases because of the rising electron Fermi energy (see Fig. 11), and it is likely that a strong temperature gradient develops, so this one-zone calculation underestimates somewhat the neutrino flux. Our calculation is also limited in that it completely neglects convection.

In Figure 12, we show the neutrino (*solid line*) and conductive (*dotted line*) fluence, as a function of time, computed with equation (5) for a fraction of carbon $X_C = 0.3$. For $X_C > 0.3$, the total conductive fluence of the burst only increases slightly; any further heating is carried off by neutrinos. For this calculation, the total radiated energy is $\approx 1.5 \times 10^{43}$ erg for a neutron star of 10 km radius—about a factor of 10 greater than that observed, although for this calculation the total energy conducted to the surface after 10^4 s is only 1.6×10^{42} erg, consistent with that measured. The evolution of the luminosity is shown in Figure 13. For such a deep layer of carbon, the thermal evolution time is quite long; the burst flux still exceeds that from accretion for several *days*, in agreement with calculations by Cumming & Bildsten (2001) for super bursts from hydrogen accreting sources.

While a one-zone approximation is tolerable at lower columns, it becomes suspect where the electrons are degenerate, since the conductivity increases with density. The electron-

---

[1]This point was also made by Cumming & Bildsten (2001) and we thank L. Bildsten for stressing this to us.

thermal conductivity is

$$\kappa = \frac{\pi^2}{3} \frac{n_e k_B^2 T}{m_e^\star} \tau \qquad (6)$$

where $\tau = p_F^2 v_F/(4\pi Z^2 e^4 n_N)\Lambda_{ei}$ is the electron-ion relaxation time. Here p_F and v_F are the electron momentum and velocity evaluated at the Fermi energy $\mathcal{E}_F$, n_e and n_N are the densities of electrons and nuclei, respectively, $m_e^\star = \mathcal{E}_F/c^2$ is the relativistic electron mass and Λ_{ei} is the Coulomb logarithm. Where relativistic, degenerate electrons dominate the pressure, the conductivity scales as $\kappa \propto Tp^{1/4}$ (neglecting variation in Λ_{ei}). Because the thermal conductivity increases with depth (pressure), heat deposited from unstable carbon burning can readily flow inwards.

To illustrate the inward flow of heat, we construct the simplest thermal transport problem by neglecting the variation of Λ_{ei}, taking the pressure to be solely that from the degenerate electrons, and writing the specific heat as $\propto k_B T/\mathcal{E}_F$ (since the electrons are more numerous than the ions, this is an adequate approximation for most of the cooling). With these simplifications, the thermal diffusion equation in non-dimensional form is

$$\frac{u}{x^{1/4}}\partial_t u - \partial_x(ux\partial_x u) = 0 \qquad (7)$$

over the domain $1 \le x \le x_R$. Here $x = y/y_\circ$, $u = T/T(y = y_\circ)$, and the time is in units of $C_p y^2/(\rho\kappa)|_{y=y_\circ}$. The flux in these units is $ux\partial_x u$. The background steady-state solution is one of constant flux,

$$u_{\text{steady}}(x, t = 0) = \left[1 + \left(2\delta u + \delta u^2\right)\frac{\ln x}{\ln x_R}\right]^{1/2}, \qquad (8)$$

where δu is the rise in temperature over the domain. To solve equation (7) numerically, we use the method of lines (PDECOL; Madsen et al. 1979), with a fifth-order polynomial spatial decomposition over logarithmically spaced collocation points and implicit integration in t. For simplicity, the temperatures at both ends of the computational domain are fixed.

At time $t = 0$ the temperature profile is u_{steady} plus a smoothed top-hat profile representing the heating injected during unstable burning. In order to investigate the transport of heat following a perturbation, we placed the boundaries at 10^9 g cm^{-2} and 10^{13} g cm^{-2} and chose the top-hat perturbation to span 1.5×10^{12} g cm$^{-2} < y < 3.5 \times 10^{12}$ g cm^{-2}, with an initial temperature of 9.1×10^9 K.

Figure 14 shows the fluence, defined here as $\int_0^t (|F| - F_S)\, dt'$, F_S being the steady-state flux, as a function of time. The solid curve denotes the fluence at the top of the layer; the dotted curve denotes that at the bottom. After 5×10^5 s, only about 0.16 of the total fluence has been radiated from the surface. The inward-directed flux will raise the temperature in

the deep ocean and crust slightly and will therefore increase the flux from the crust above the ≈ 0.1 MeV $N_A \dot{m}$ long-term value. While all of the heat deposited in the ocean will eventually be radiated from the surface, only the fraction that is radiated immediately following the burst is discernible in the X-ray lightcurve. As in Figure 12, the evolution timescale is roughly the thermal timescale at the base of the heated layer.

This simple calculation is only meant to be illustrative: it ignores neutrino cooling and in particular it underestimates the thermal transport to the surface. A convective layer develops during the burst (Taam & Picklum 1978); this convection may be enhanced by the stronger neutrino emissivity at lower densities (Fig. 11). To reproduce correctly the burst evolution and the lightcurve requires an implicit evolution code, which is beyond the scope of this paper; for now we note that the total fluence of the super burst is systematically underestimated, by perhaps as much as an order of magnitude.

For both cooling calculations (eqs. [5] and [7]), only a small fraction of the burst energy is radiated away after 10^4 s. *As a result, the fluence observed during the three hours following the burst is consistent with the burning of a large mass of carbon at great depth.* The strongest constraint on this scenario is the recurrence time: to accrete a column of 10^{13} g cm^{-2} takes $13.3/(\dot{M}/3 \times 10^{17}$ g s$^{-1})$ yr.

5. Discussion and Summary

Thermonuclear bursts provide a unique probe of the physics of neutron stars. Their properties depend on the accretion rate and composition of the accreted matter, the bulk properties of neutron stars, the thermal state of the neutron star and the detailed nuclear burning physics. 4U 1820-30 is an especially revealing system since its extreme properties place strong constraints on the composition of the accreted matter. The observation of a super burst from 4U 1820-30 with $> 1,000$ times the energy release of a typical helium burst provides us with a compelling look at processes occurring at much greater depth in the neutron star "ocean" than we are normally privileged to witness.

We have investigated the ignition of a ^{12}C-rich layer, presumably produced during the high-luminosity state when no type I X-ray bursts are observed. When the mass of this layer is $\gtrsim 10^{26}$ g, a thermal runaway ensues. Unlike the case discussed by Cumming & Bildsten (2001), the lack of heavy rp-process ashes makes the carbon layer cooler for this source and a larger mass of carbon is required for ignition. Once the runaway begins, the temperature rises to $\sim 10^{10}$ K. The burning ends and the layer rapidly cools by neutrino emission until the temperature is $\sim 5 \times 10^9$ K, at which point thermal conduction becomes more efficient

at cooling the layer. Because of the great depth of the ignition, heat readily flows inward, and the temperature evolves on a timescale $\sim 10^5$ s. As a result, the measured X-ray fluence is only a small fraction of the total, so that this scenario is consistent with the observation. The recurrence time would provide a strong constraint on the ignition column. To accrete an ignition column of 10^{13} g cm^{-2} takes $\sim 13/(\dot{M}/3 \times 10^{17}$ g s$^{-1})$ yr. If the accretion rate were much higher than that inferred by the X-ray luminosity, than the ocean would be hotter, and the ignition column reduced. Recurrence times of less than a year would require that $\dot{M} > 10^{18}$ g cm^{-2}, however, or that the ignition be prematurely triggered.

As noted by Cumming & Bildsten (2001), the heating from this burst can quench type I X-ray bursts until the cooling luminosity is $\approx 0.01 L_{\mathrm{accr}}$ (Bildsten 1995). If the scenario we outline is correct, then no type I X-ray bursts should have occurred in the week following the super burst. Distinguishing the elevated flux following the burst will be more difficult, given the variability of the accretion flux. The strongest constraint on this scenario would be if another super burst were detected after a timescale much less than a decade. This would suggest that the carbon ignition is triggered. The fact that a He burst occurred immediately prior to the super burst is intriguing; if the carbon ignition did occur at large densities, then the thermal instability began several hours prior to the observed rise of the burst. It is possible that the flux from the carbon runaway could ignite any accumulated He.

While the calculations presented here are suggestive, they are very crude and could be substantially improved. Evolutionary calculations, with reaction networks, of the ignition and subsequent evolution of this burst, coupled with similar calculations for the super bursts seen from hydrogen accreting sources, can inform us about the relevant physics at work in the deep ocean. Continued X-ray monitoring of the source should eventually give a better constraint on the recurrence time. An important quantity is the amount of carbon produced; for the scenario we outline here to work, roughly half of the accreted matter must burn to carbon so that the ignition is indeed unstable.

The X-ray spectrum during the burst reveals a broad emission line indicative of Fe $K\alpha$ fluorescence as well as an absorption edge in the 7–9 keV range. The very high signal-to-noise spectra obtained during the burst make the detection of these discrete features extremely secure. Previous authors have predicted that such features might be produced by disk reflection (see for example Day & Done 1991), but to our knowledge this is the first confident detection. Detailed modeling of these features could provide a new probe of the accretion disk in bursting systems. Here we have only scratched the surface in terms of investigating the discrete components. An in-depth study and interpretation of the line and edge will be presented in a future publication.

REFERENCES

Anderson, S. F., Margon, B., Deutsch, E. W., Downes, R. A., & Allen, R. G. 1997, ApJ, 482, L69

Arons, J. & King, I. R. 1993, ApJ, 413, L121

Bildsten, L. 1995, ApJ, 438, 852

Bildsten, L. 1998, in The Many Faces of Neutron Stars, ed. A. Alpar, R. Buccheri, & J. van Paradijs, Vol. 515, NATO ASI ser. C (Dordrecht: Kluwer), 419

Bildsten, L. 2000, in Cosmic Explosions, ed. S. S. Holt & W. W. Zhang

Bisnovatyi-Kogan, G. S. & Chechetkin, V. M. 1979, Soviet Phys.-Uspekhi, 127, 263

Blaes, O., Blandford, R., Madau, P., & Koonin, S. 1990, ApJ, 363, 612

Brown, E. F. 2000, ApJ, 531, 988

Brown, E. F. & Bildsten, L. 1998, ApJ, 496, 915

Brown, E. F., Bildsten, L., & Rutledge, R. E. 1998, ApJ, 504, L95

Buchler, J. R. & Yueh, W. R. 1976, ApJ, 210, 440

Caughlan, G. R. & Fowler, W. A. 1988, At. Data Nucl. Data Tables, 40, 283

Clark, G. W., Li, F. K., Canizares, C., Hayakawa, S., Jernigan, G., & Lewin, W. H. G. 1977, MNRAS, 179, 651

Cornelisse, R., Heise, J., Kuulkers, E., Verbunt, F., & in't Zand, J. J. M. 2000, ApJ, 357, L21

Cumming, A. & Bildsten, L. 2001, ApJ, submitted, (astro-ph/0107213)

Day, C. S. R. & Done, C. 1991, MNRAS, 253, 35P

Ebisuzaki, T. 1987, PASJ, 39, 287

Ebisuzaki, T. & Nakamura, N. 1988, ApJ, 328, 251

Farouki, R. & Hamaguchi, S. 1993, Phys. Rev. E, 47, 4330

Foster, A. J., Fabian, A. C., & Ross, R. R. 1987, MNRAS, 228, 259

Franco, L. M. & Strohmayer, T. E. 1999, in American Astronomical Society Meeting, Vol. 195, 12609

Fryxell, B. A. & Woosley, S. E. 1982, ApJ, 258, 733

Fushiki, I. & Lamb, D. Q. 1987, ApJ, 317, 368

Grindlay, J. & Gursky, H. 1976, ApJ, 205, L131

Haberl, F., Stella, L., White, N. E., Gottwald, M., & Priedhorsky, W. C. 1987, ApJ, 314, 266

Haberl, F. & Titarchuk, L. 1995, A&A, 299, 414

Haensel, P. & Zdunik, J. L. 1990, A&A, 227, 431

Hansen, C. J. & Van Horn, H. M. 1975, ApJ, 195, 735

Heise, J., in't Zand, J. J. M., & Kuulkers, E. 2000, AAS/High Energy Astrophysics Division, 32, 2803+

Hesser, J. E. & Shawl, S. J. 1985, PASP, 97, 465

Hoffman, J. A., Lewin, W. H. G., Doty, J., Jernigan, J. G., Haney, M., & Richardson, J. A. 1978, ApJ, 221, L57

Inogamov, N. A. & Sunyaev, R. A. 1999, Astronomy Letters, 25, 269

Itoh, N., Hayashi, H., Nishikawa, A., & Kohyama, Y. 1996, ApJS, 102, 411

Itoh, N., Kuwashima, F., Ichihashi, K., & Mutoh, H. 1991, ApJ, 382, 636

Joss, P. C. & Li, F. K. 1980, ApJ, 238, 287

Kaaret, P., Ford, E. C., & Chen, K. 1997, ApJ, 480, L27

Kuulkers, E. 2001, Ast. Tel., 68, 1

Lewin, W. H. G., Vacca, W. D., & Basinska, E. M. 1984, ApJ, 277, L57

Li, Y., Gu, M. F. & Kahn, S. M. 2001, ApJ, submitted, (astro-ph/0106163)

Litwin, C., Brown, E. F., & Rosner, R. 2001, ApJ, 533, 788

London, R. A., Taam, R. E., & Howard, W. M. 1986, ApJ, 306, 170

Madej, J. 1997, A&A, 320, 177

Madej, J. 1991, ApJ, 376, 161

Madej, J. 1989, ApJ, 339, 386

Madsen, N. K., , & Sincovec, R. F. 1979, ACM Trans. Math. Soft., 5, 326

Magnier, E., Lewin, W. H. G., van Paradijs, J., Tan, J., Penninx, W., & Damen, E. 1989, MNRAS, 237, 729

Nakamura, N., Inoue, H., & Tanaka, Y. 1988, PASJ, 40, 209

Nayakshin, S., Kallman, T. R. 2001, ApJ, 546, 406

Ogata, S., Ichimaru, S., & van Horn, H. M. 1993, ApJ, 417, 265

Popham, R. & Sunyaev, R. 2001, ApJ, 547, 355

Potekhin, A. Y., Baiko, D. A., Haensel, P., & Yakovlev, D. G. 1999, A&A, 346, 345

Potekhin, A. Y., Chabrier, G., & Yakovlev, D. G. 1997, A&A, 323, 415

Priedhorsky, W. & Terrell, J. 1984, ApJ, 284, L17

Rappaport, S., Ma, C. P., Joss, P. C., & Nelson, L. A. 1987, ApJ, 322, 842

Rich, R. M., Minniti, D., & Liebert, J. 1993, ApJ, 406, 489

Ross, R. R., Fabian, A. C. & Young, A. J. 1999, MNRAS, 306, 461

Sampson, D. H. 1959, ApJ, 129, 734

Schatz, H., Aprahamian, A., Barnard, V., Bildsten, L., Cumming, A., Ouellette, M., Rauscher, T., Thielemann, F.-K., & Wiescher, M. 2001, Phys. Rev. Lett., in press

Schatz, H., Bildsten, L., Cumming, A., & Wiescher, M. 1999, ApJ, 524, 1014

Smale, A. P., Zhang, W., & White, N. E. 1997, ApJ, 483, L119

Spitkovsky, A., Levin, Y., & Ushomirsky, G. 2001, ApJ, submitted. preprint available: astro-ph/0108074

Stella, L., White, N. E., & Priedhorsky, W. 1987, ApJ, 312, L17

Strohmayer, T. E. 2000, AAS/High Energy Astrophysics Division, 32, 2410

Taam, R. E. & Picklum, R. E. 1978, ApJ, 224, 210

Tawara, Y., Kii, T., Hayakawa, S., Kunieda, H., Masai, K., Nagase, F., Inoue, H., Koyama, K., Makino, F., Makishima, K., Matsuoka, M., Murakami, T., Oda, M., Ogawara, Y., Ohashi, T., Shibazaki, N., Tanaka, Y., Miyamoto, S., Tsunemi, H., Yamashita, K., & Kondo, I. 1984, ApJ, 276, L41

Timmes, F. X. & Swesty, F. D. 2000, ApJS, 126, 501

Timmes, F. X. & Woosley, S. E. 1992, ApJ, 396, 649

Titarchuk, L. 1994, ApJ, 429, 340

Townsend, A. A. 1966, J. Fluid Mech., 1, 29

Turner, T. J., Done, C., Mushotzky, R., Madejski, G. & Kunieda, H. 1992, ApJ, 391, 102

Urpin, V. A. & Yakovlev, D. G. 1980, Soviet Ast., 24, 126

Vacca, W. D., Lewin, W. H. G., & van Paradijs, J. 1986, MNRAS, 220, 339

van Paradijs, J., Dotani, T., Tanaka, Y., & Tsuru, T. 1990, PASJ, 42, 633

Waki, I., Inoue, H., Koyama, K., Matsuoka, M., Murakami, T., Ogawara, Y., Ohashi, T., Tanaka, Y., Hayakawa, S., Tawara, Y., Miyamoto, S., Tsunemi, H., & Kondo, I. 1984, PASJ, 36, 819

Walker, M. A. & Meszaros, P. 1989, ApJ, 346, 844

Wijnands, R. 2001, ApJ, 554, L59

Woosley, S. E. & Taam, R. E. 1976, Nature, 263, 101

Youngs, D. L. 1994, Lasers and Particle Beams, 12, 725

Zhang, W., Strohmayer, T. E., & Swank, J. H. 1997, ApJ, 482, L167

Zingale, M., Timmes, F. X., Fryxell, B., Lamb, D. Q., Olson, K., Calder, A. C., Dursi, L. J., Ricker, P., Rosner, R., MacNeice, P., & Tufo, H. M. 2001, ApJS, in press

6. Figure Captions
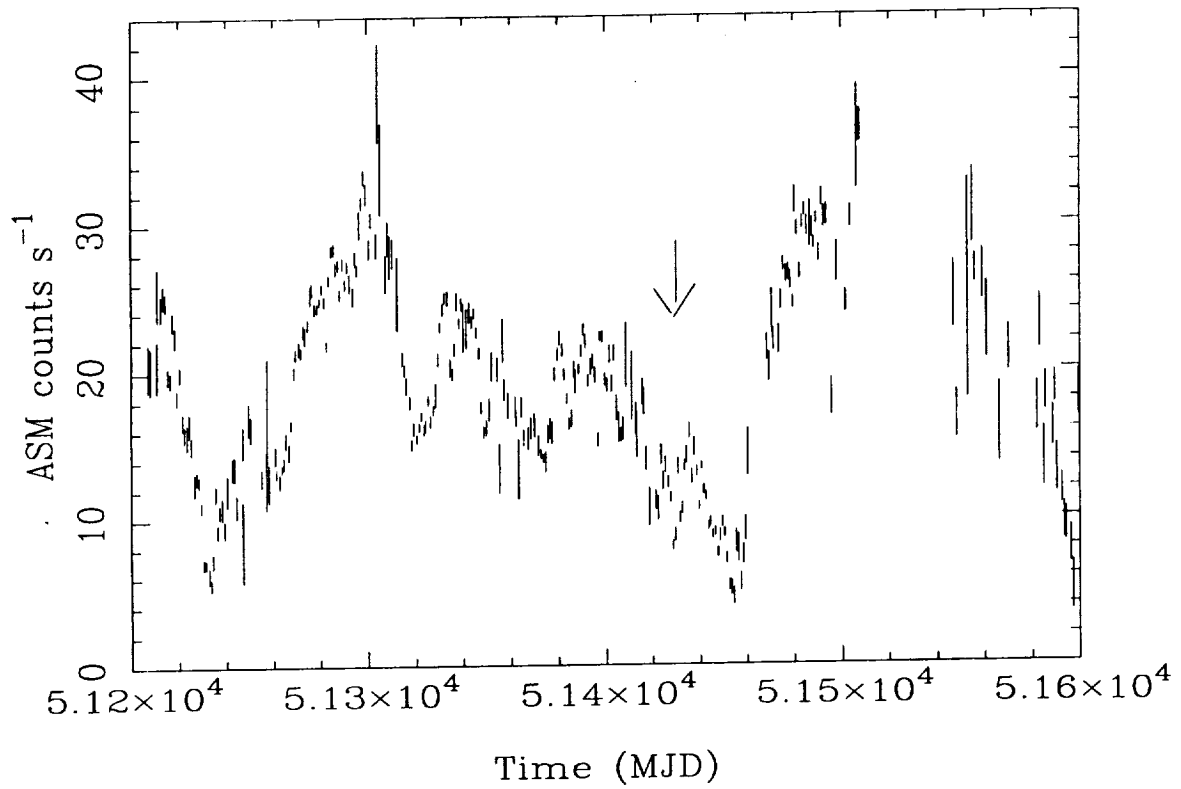
Fig. 1.— RXTE/ASM lightcurve of 4U 1820-30 prior to and around the epoch of the super burst. A flux of 1 Crab is approximately 75 ASM units.

Fig. 2.— Time history of the X-ray flux from 4U 1820-30 during the super burst. The PCA lightcurve (2 - 90 keV) at 1/8 s resolution is the higher time resolution trace (left axis). The lower time resolution curve is the (8 - 30)/(2 - 8) keV hardness ratio from Standard2 data with 16 s resolution (right axis).

Fig. 3.— Comparison of the helium flash which preceded the super burst (top panel) and a helium flash which was observed on May 2, 1997 (bottom panel). Shown for both bursts are the 2 - 90 keV lightcurves from Standard1 data with 1/8 s time resolution.

Fig. 4.— Derived bremsstrahlung temperatures (top panel) and 2 - 20 keV fluxes (bottom panel) for the persistent, accretion driven flux prior to the super burst.

Fig. 5.— Residuals to a spectral fit during the peak of the burst using a black body function with photoelectric absorption. Shown are the residuals, data - model, in units of standard deviations. The emission line feature just longward of 6 keV as well as the edge between 8 - 10 keV are cleary evident.

Fig. 6.— Count rate spectrum and model (top panel) and residuals, data - model in units of standard deviations (bottom panel) for a spectral fit to an interval during the peak of the burst. The model includes a black body function, a gaussian emission line near 6 kev and an absorption edge near 9 keV. Note that the error bars near the peak of the spectrum are almost smaller than the width of the lines.

Fig. 7.— Lightcurve of the burst from Standard1 data on a linear time axis. The dashed vertical lines denote the region in which we investigated the spectral evolution during the burst.

Fig. 8.— Time evolution of the bolometric flux (top panel), black body temperature (middle) and the inferred black body radius (bottom) assuming a distance of 6.6 kpc. The time interval shown corresponds to the interval between the vertical dashed lines in figure 7. The bolometric flux was derived by integrating the best-fit black body spectrum.

Fig. 9.— Time evolution of the emission line and absorption edge components throughout the burst. Shown are the line centroid energy, and line flux from the diskline model (top and 2nd from top) along with the edge energy and depth (bottom and next to bottom) from the smedge model.

Fig. 10.— The thermal structure of the other layers of a neutron star accreting pure He at a local accretion rate $\dot{m} = 2.25 \times 10^4$ g cm^{-2} s^{-1}. The top axis indicates the time required for a column y to be accreted at this rate. Plotted are the temperature (*solid line*) and flux (*dotted line*) in units of MeV per accreted nucleon. The arrow is to guide the eye to the value of T at $y = 10^{14}$ g cm^{-2}. The dots indicates the base of the C/Fe layer. The condition for instability of the reaction ^{12}C + ^{12}C is indicated by the heavy dashed curve.

Fig. 11.— The neutrino emissivity at a temperature of 10^{10} K, as function of column for a surface gravity 2.34×10^{14} cm s^{-1}.

Fig. 12.— The fluence, in units of 10^{28} erg cm^{-2}, as a function of time, in units of 10^4 s, for the one-zone calculation (eq. [5]). Shown are both the neutrino (*solid line*) and conductive (*dotted line*) fluences. The conductive flux evolves on the thermal diffusion timescale appropriate for a depth of $y = 10^{13}$ g cm^{-2}.

Fig. 13.— The luminosity, in units of 10^{38} erg s^{-1}, as a function of time, in units of 10^4 s, for the one-zone calculation (eq. [5]).

Fig. 14.— The conductive fluence, in units of 10^{28} erg cm^{-2}, for the model calculation described in eq. [7], as a function of time in units of 10^4 s. We show both the outward-directed (*solid line*) and inward-directed (*dotted line*) fluence. As in Fig. 12, the evolution of the fluence is on the thermal decay timescale at the base of the burning layer.

Figure 1: RXTE/ASM lightcurve of 4U 1820-30 prior to and around the epoch of the super burst. A flux of 1 Crab is approximately 75 ASM units.
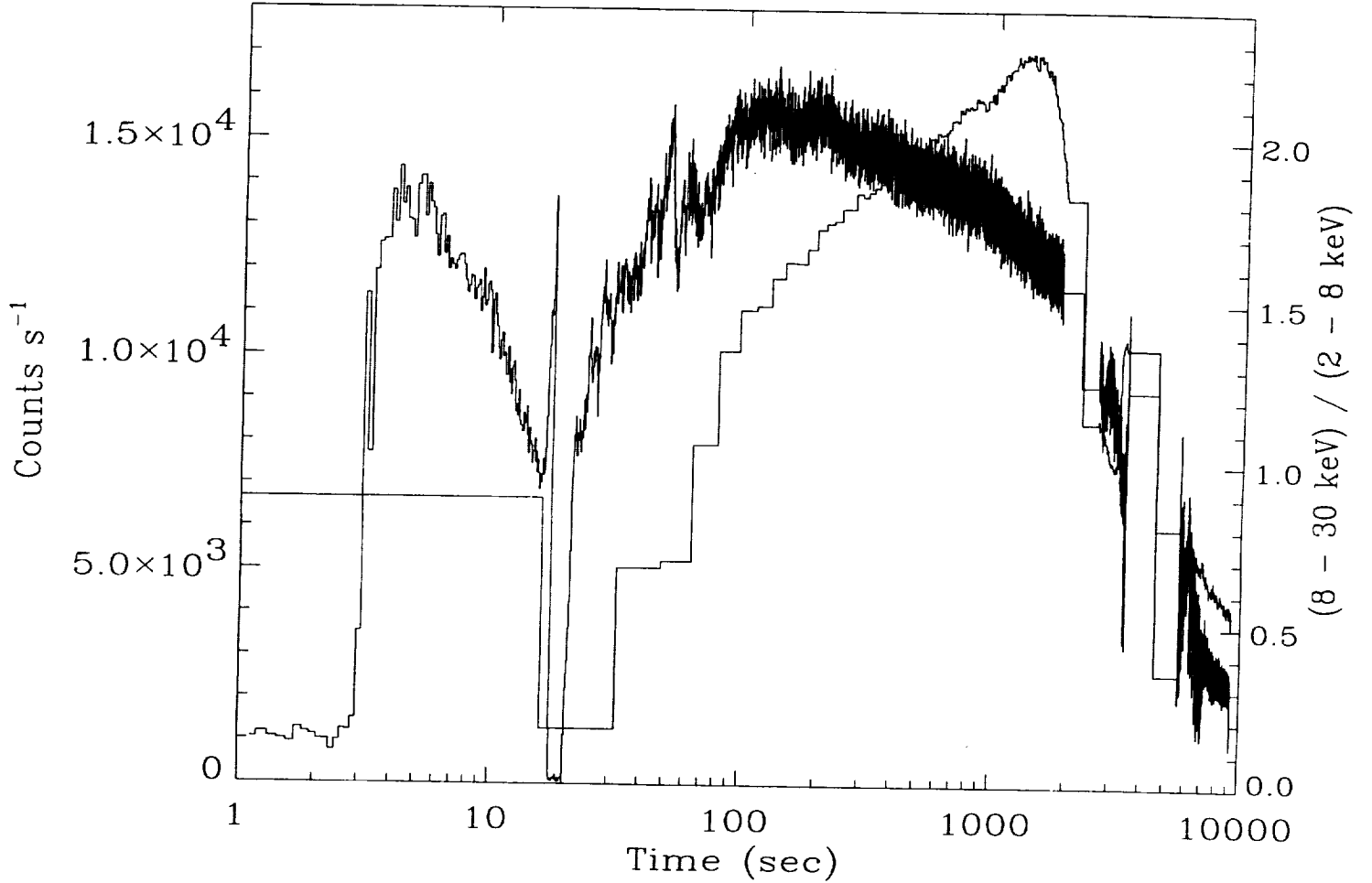
Figure 2: Time history of the X-ray flux from 4U 1820-30 during the super burst. The PCA lightcurve (2 - 60 keV) at 1/8 s resolution is the higher time resolution trace (left axis). The lower time resolution curve is the (8 - 30)/(2 - 8) keV hardness ratio from Standard2 data with 16 s resolution (right axis).
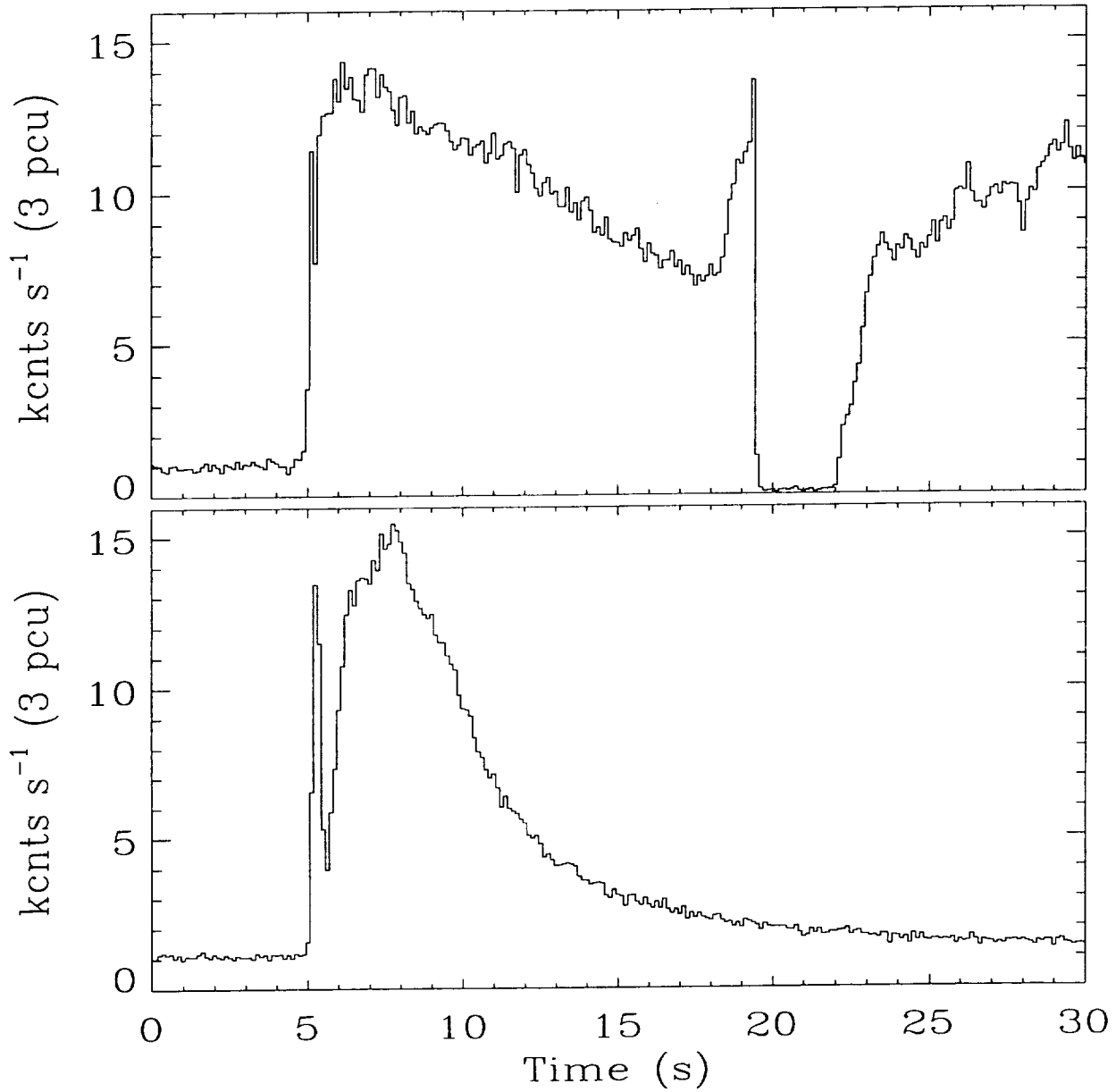
Figure 3: Comparison of the helium flash which preceded the super burst (top panel) and a helium flash which was observed on May 2, 1997 (bottom panel). Shown for both bursts are the 2 - 60 keV lightcurves from Standard1 data with 1/8 s time resolution. The rates are scaled to 3 PCU detectors.
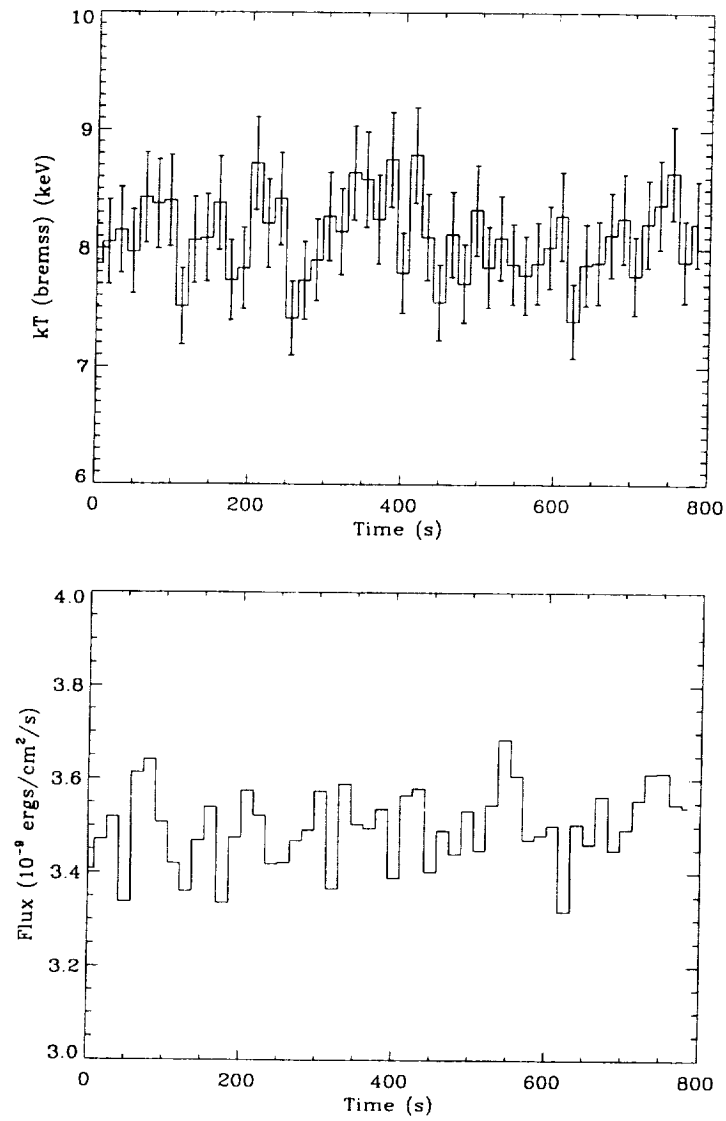
Figure 4: Derived bremsstrahlung temperatures (top panel) and 2 - 20 keV fluxes (bottom panel) for the persistent, accretion driven flux prior to the super burst.
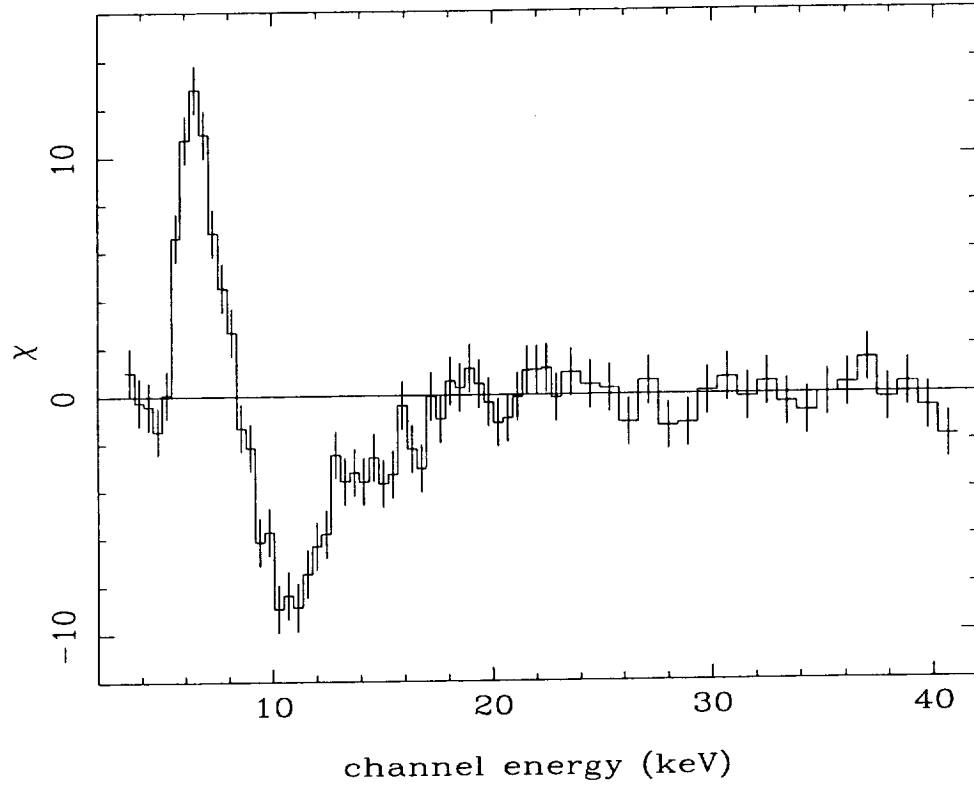
Figure 5: Residuals to a spectral fit during the peak of the burst using a black body function with photoelectric absorption. Shown are the residuals, data - model, in units of standard deviations. The emission line feature just longward of 6 keV as well as the edge between 8 - 10 keV are cleary evident.
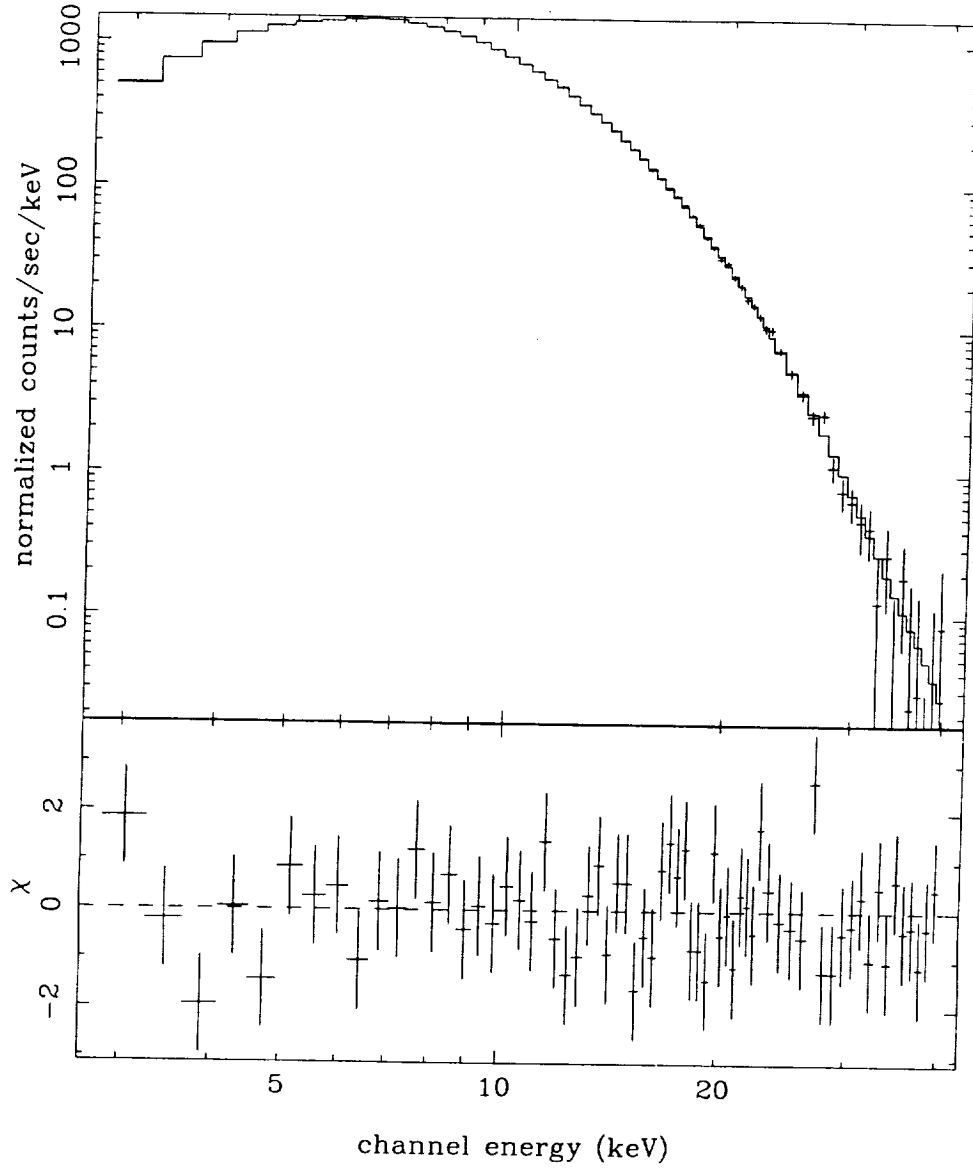
Figure 6: Count rate spectrum and model (top panel) and residuals, data - model in units of standard deviations (bottom panel) for a spectral fit to an interval during the peak of the burst. The model includes a black body function, a gaussian emission line near 6 kev and an absorption edge near 9 keV. Note that the error bars near the peak of the spectrum are almost smaller than the width of the lines.
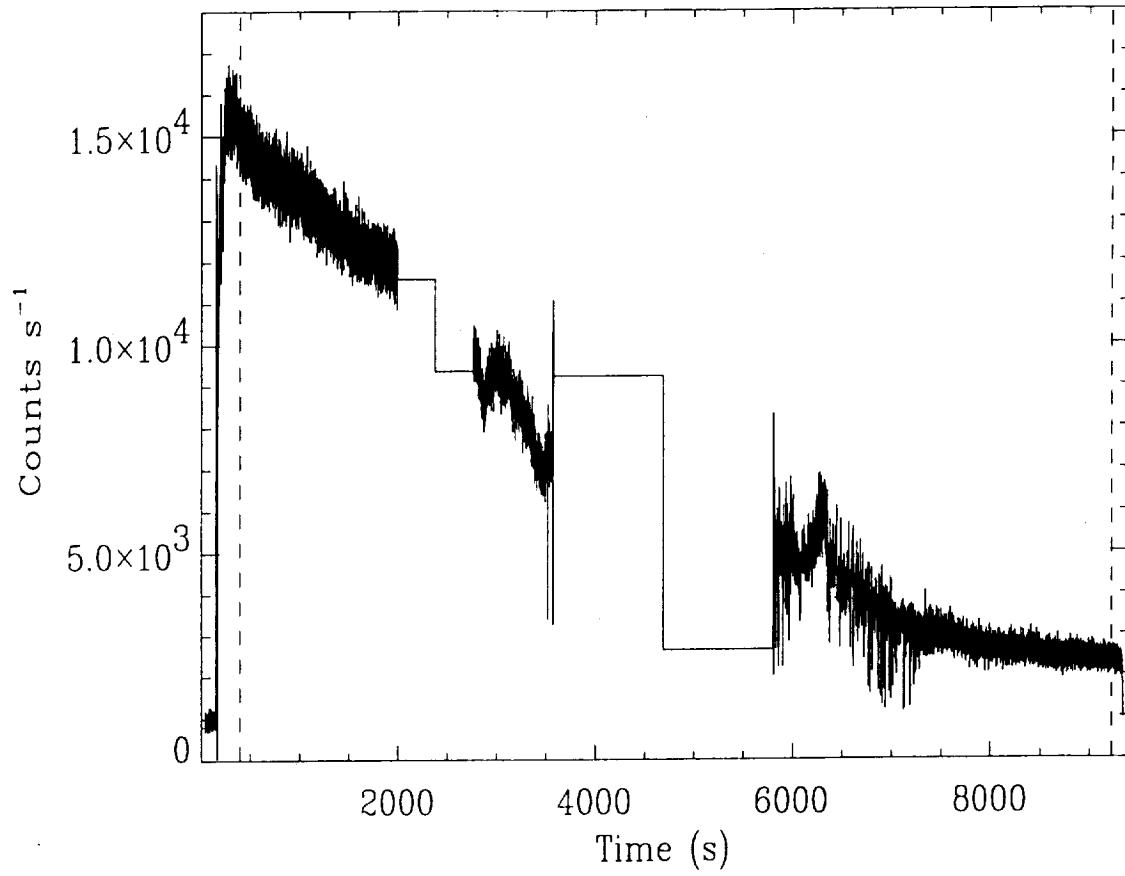
Figure 7: Lightcurve of the burst from Standard1 data on a linear time axis. The dashed vertical lines denote the region in which we investigated the spectral evolution during the burst.
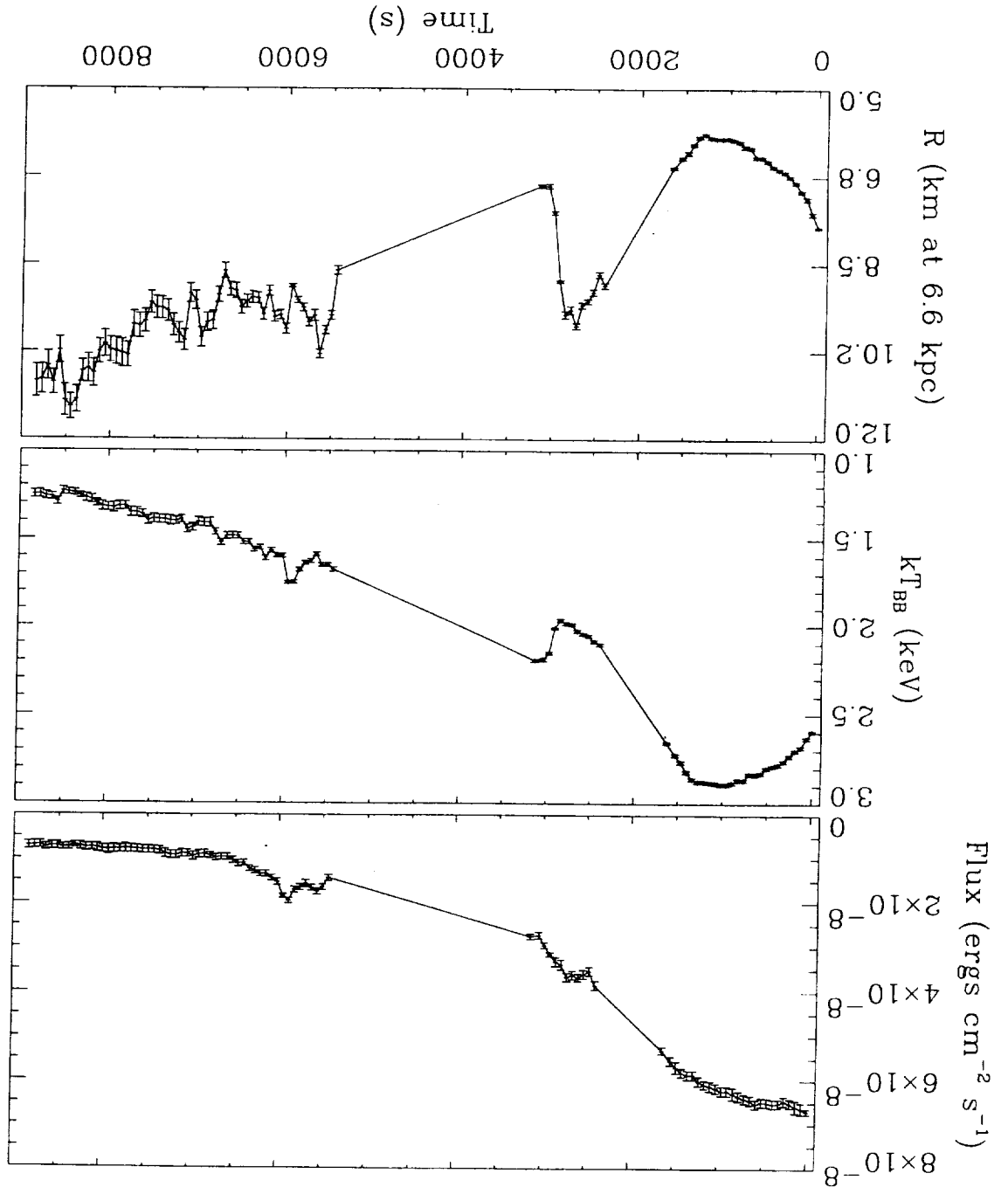
Figure 8: Time evolution of the bolometric flux (top panel), black body temperature (middle) and the inferred black body radius (bottom) assuming a distance of 6.6 kpc. The time interval shown corresponds to the interval between the vertical dashed lines in figure 7. The bolometric flux was derived by integrating the best-fit black body spectrum.
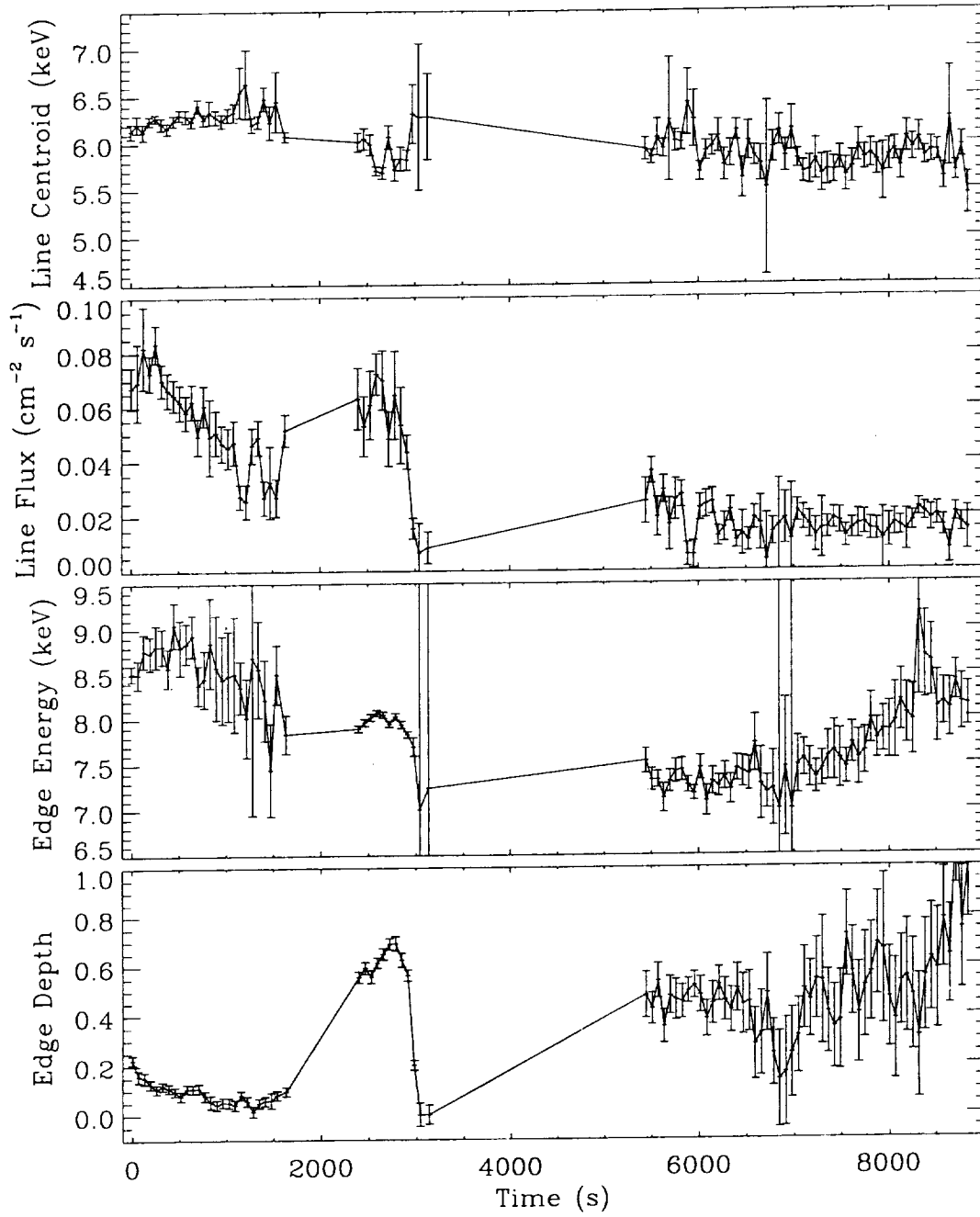
Figure 9: Time evolution of the emission line and absorption edge components throughout the burst. Shown are the line centroid energy, and line flux from the diskline model (top and 2nd from top) along with the edge energy and depth (bottom and next to bottom) from the smedge model.
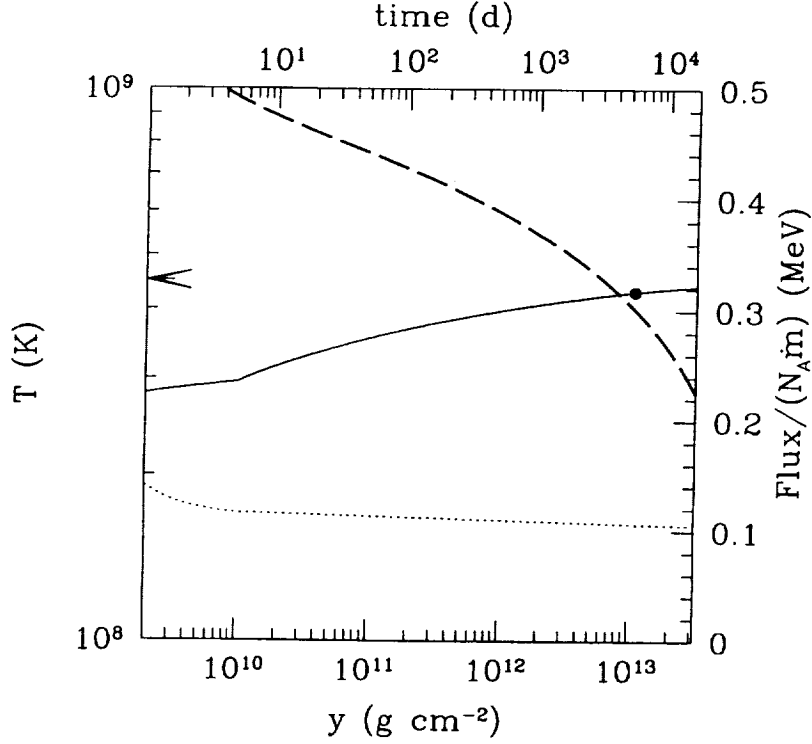
Figure 10: The thermal structure of the other layers of a neutron star accreting pure He at a local accretion rate $\dot{m} = 2.25 \times 10^4$ g cm^{-2} s^{-1}. The top axis indicates the time required for a column y to be accreted at this rate. Plotted are the temperature (*solid line*) and flux (*dotted line*) in units of MeV per accreted nucleon. The arrow is to guide the eye to the value of T at $y = 10^{14}$ g cm^{-2}). The dots indicates the base of the C/Fe layer. The condition for instability of the reaction ^{12}C + ^{12}C is indicated by the heavy dashed curve.
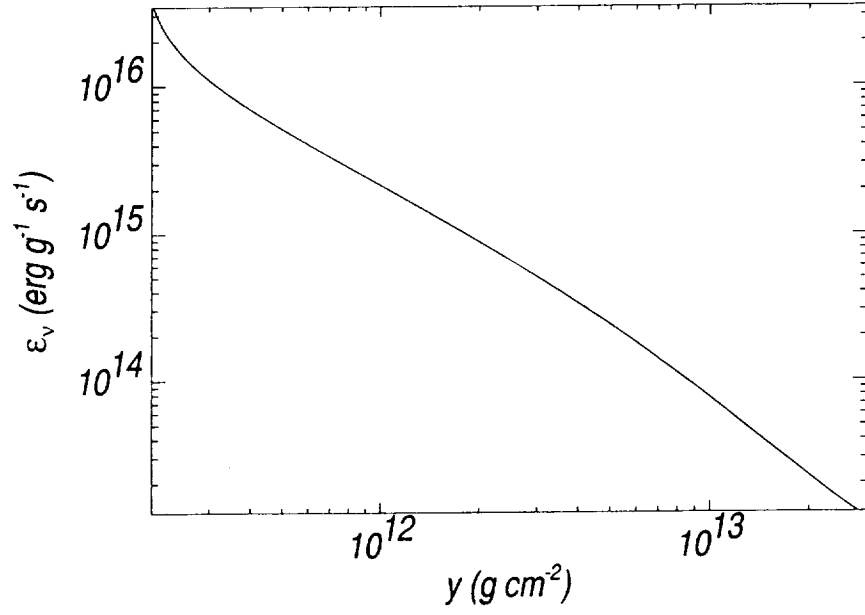
Figure 11: The neutrino emissivity at a temperature of 10^{10} K, as function of column for a surface gravity 2.34×10^{14} cm s^{-1}.
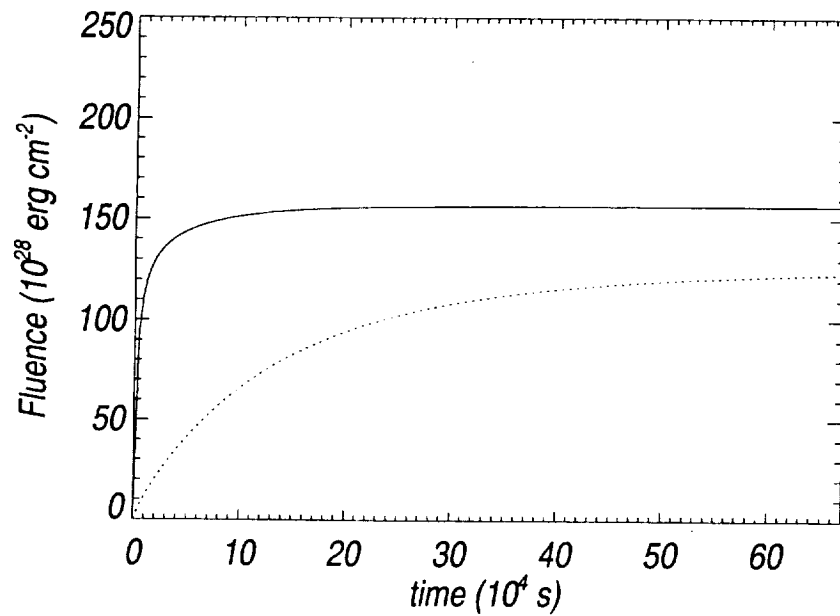
Figure 12: The fluence, in units of 10^{28} erg cm^{-2}, as a function of time, in units of 10^4 s, for the one-zone calculation (eq. [5]). Shown are both the neutrino (*solid* line) and conductive (*dotted* line) fluences. The conductive flux evolves on the thermal diffusion timescale appropriate for a depth of $y = 10^{13}$ g cm^{-2}.
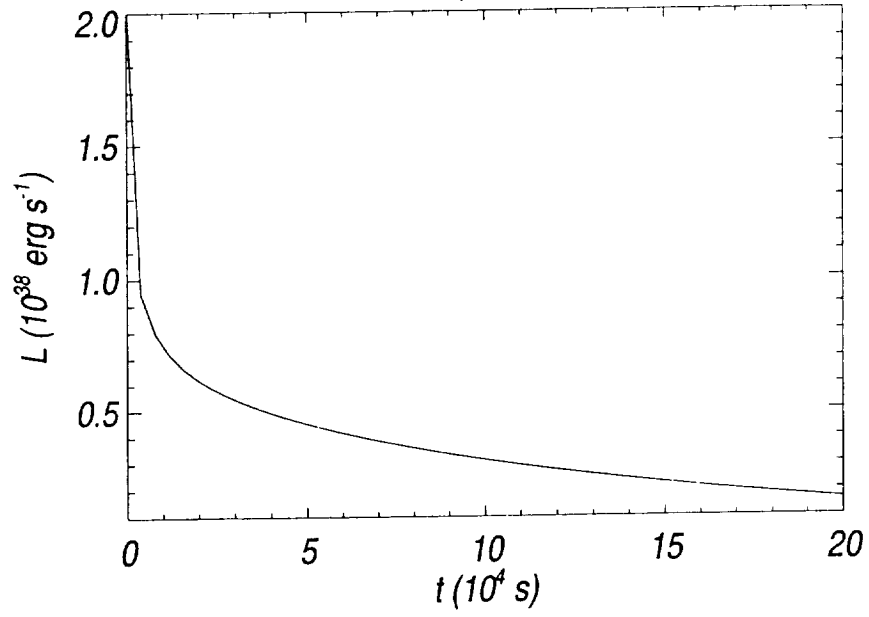
Figure 13: The luminosity, in units of 10^{38} erg s^{-1}, as a function of time, in units of 10^4 s, for the one-zone calculation (eq. [5]).
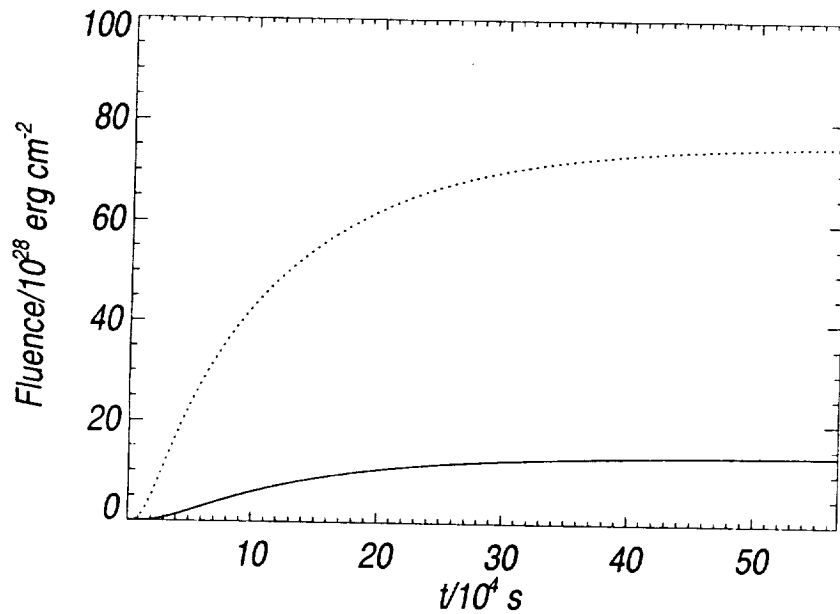
Figure 14: The conductive fluence, in units of 10^{28} erg cm^{-2}, for the model calculation described in eq. [7], as a function of time in units of 10^4 s. We show both the outward-directed (*solid* line) and inward-directed (*dotted* line) fluence. As in Fig. 12, the evolution of the fluence is on the thermal decay timescale at the base of the burning layer.